AD-A176 941 HIGH POWER MICROWAVE BREAKDOWN EXPERIMENTAL DESIGN STUDY(U) TRW ELECTRONICS AND DEFENSE SECTOR REDONDO BEACH CA W F DIVERGILIO ET AL. FEB 82 SBI-AD-E001 309 1/1

UNCLASSIFIED N00173-80-C-0476 F/G 20/14 NL

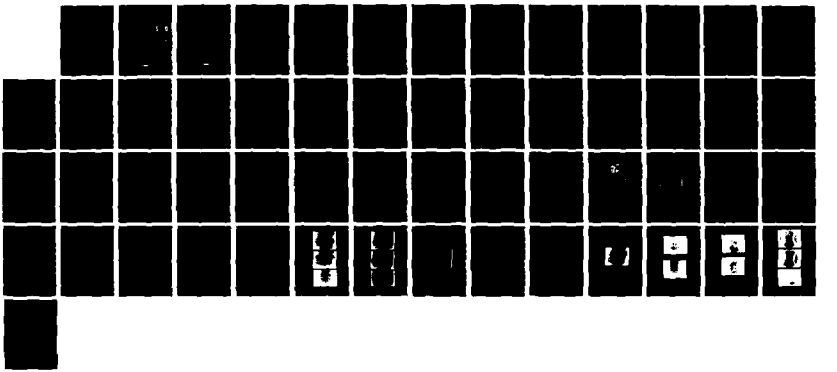

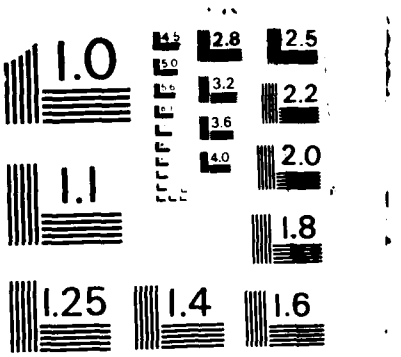

HIGH POWER MICROWAVE BREAKDOWN EXPERIMENTAL DESIGN STUDY

PREPARED FOR

NAVAL RESEARCH LABORATORY
CONTRACT NO. N00173-80-C-0476

BY
WILLIAM F. DIVERGILIO
JEFFREY J. THOMSON

FINAL REPORT
FEBRUARY 1982

TRW
DEFENSE AND SPACE SYSTEMS GROUP

HIGH POWER MICROWAVE BREAKDOWN EXPERIMENTAL DESIGN STUDY

PREPARED FOR

NAVAL RESEARCH LABORATORY

CONTRACT NO. N00173-80-C-0476

APPROVED FOR PUBLIC RELEASE
DISTRIBUTION UNLIMITED

BY

WILLIAM F. DIVERGILIO

JEFFREY J. THOMSON

FINAL REPORT
FEBRUARY 1982

TRW
DEFENSE AND SPACE SYSTEMS GROUP

Unclassified

SECURITY CLASSIFICATION OF THIS PAGE (When Data Entered)

REPORT DOCUMENTATION PAGE		READ INSTRUCTIONS BEFORE COMPLETING FORM
1. REPORT NUMBER	2. GOVT ACCESSION NO. AD-A176 941	3. RECIPIENT'S CATALOG NUMBER
4. TITLE (and Subtitle) High Power Microwave Breakdown Experimental Design Study		5. TYPE OF REPORT & PERIOD COVERED Final 80 Sept 25 - 81 Oct 25
		6. PERFORMING ORG. REPORT NUMBER
7. AUTHOR(s) William F. DiVergilio Jeffrey J. Thomson		8. CONTRACT OR GRANT NUMBER(s) N00173-80-C-0476
9. PERFORMING ORGANIZATION NAME AND ADDRESS TRW Electronics and Defense One Space Park Redondo Beach, CA 90278		10. PROGRAM ELEMENT, PROJECT, TASK AREA & WORK UNIT NUMBERS
11. CONTROLLING OFFICE NAME AND ADDRESS Contracting Office Naval Research Laboratory Washington, D.C. 20375		12. REPORT DATE 82 February
		13. NUMBER OF PAGES
14. MONITORING AGENCY NAME & ADDRESS (if different from Controlling Office) AFPRO TRW One Space Park Redondo Beach, CA 90278		15. SECURITY CLASS. (of this report) Unclassified
		15a. DECLASSIFICATION/DOWNGRADING SCHEDULE

16. DISTRIBUTION STATEMENT (of this Report)

APPROVED FOR PUBLIC RELEASE
DISTRIBUTION UNLIMITED

17. DISTRIBUTION STATEMENT (of the abstract entered in Block 20, if different from Report)

18. SUPPLEMENTARY NOTES

19. KEY WORDS (Continue on reverse side if necessary and identify by block number)
Microwave Breakdown

20. ABSTRACT (Continue on reverse side if necessary and identify by block number)
A series of experiments, and necessary apparatus, designed to study phenomenae associated with microwave breakdown in front of a conducting surface is suggested. The design utilizes conventional microwave sources, allowing study of breakdown up to an ambient of about half an atmosphere. A simple model for breakdown in front of a conducting surface, including electron density growth and saturation and microwave absorption, is described, and experiments designed to test the model are discussed. Results obtained from preliminary experiments performed under a TRW IR&D program are also described. These results

DD FORM 1 JAN 73 1473 EDITION OF 1 NOV 65 IS OBSOLETE

Unclassified

SECURITY CLASSIFICATION OF THIS PAGE (When Data Entered)

20. Continued...

qualitatively verify the model predictions of high microwave absorption, and also illustrate some of the more complex phenomenae associated with microwave breakdown, including shock wave generation and filamentation.

TABLE OF CONTENTS

1. INTRODUCTION

The aim of this study was the development of a series of experiments addressing the key physics issues of microwave breakdown in the parameter regime of interest for the Navy High Power Microwave Breakdown program. The particular geometry considered was breakdown in the maxima of the standing electromagnetic wave pattern produced by microwave reflection from a conducting surface. Navy interest focusses on breakdown at or near atmospheric pressure over spatial scale lengths large compared to the microwave wavelength. Experiments in this regime will require sources with total output powers on the order of hundreds of megawatts. The major constraint we have placed on this design study is that readily available, conventional microwave sources be employed in the experiments. While this constraint makes large scale, full atmosphere experiments inaccessible, it does remove any dependence of the program on advanced source development, thus facilitating the more rapid development of a physics data base. Results obtained in the scaled experiments can then provide timely input for future direction of source development programs.

The basic theory of breakdown and microwave absorption near a conducting surface is described in Section 2 and in more detail in Appendices A and B. The theory as developed here described the basic physics of breakdown and microwave absorption, but only for the one dimensional case with breakdown only at the first peak of the standing wave pattern. Following experimental validation of the basic theory, multiple breakdown regions and two or three dimensional phenomenae such as filamentation should be included in the theory.

In Section 3 we outline a series of experiments designed to first test the basic theory and then extend investigations into areas of more complex phenomenae. The suggested experiments are largely based on preliminary experiments carried out under the TRW Microwave Breakdown IR&D program, described in Appendix C. The experimental apparatus, which is based on the apparatus used in the IR&D program, is described in Section 4. The area requiring the most future development is diagnostics of the breakdown region. In the course of this study, a number of potential diagnostic techniqes were tested, with varying degrees of success, on the IR&D experimental setup. Dicussion of these diagnostics can be found in Section 3 and 4 and Appendix C.

2. THEORETICAL STUDIES

The major areas of theoretical interest in this problem are:

(1) Absorption of the incident radiation
(2) Plasma formation and the approach to a steady state
(3) Radiation
(4) Shock formation

A complete description of the theoretical model is given in Appendix A. Here we describe the essential results in each of the above areas.

2.1 ABSORPTION

Figure 1 shows the model used for absorption for a single breakdown region. Multiple regions would require a straight forward extension of this analysis. The plasma is assumed to be a uniform dielectric (dielectric constant $\varepsilon = 1 - \omega_p^2/\omega(\omega+i\nu)$ of a width L, located at the first peak of the standing wave pattern. The target is a perfect conductor. The absorption is

$$f = \frac{4\ Im(AB^*)}{|A^2| + |B^2| + 2\ Im(AB^*)} \tag{1}$$

where A and B are defined in the appendix. For a thin plasma,

$$f = 4\ (Im\varepsilon)k_o L \tag{2}$$

This would be the usual result for a plane wave passing through a dielectric, except for the factor of 4 which results from the standing wave enhancement.

The unknown parameters, which are determined self-consistently are ω_p^2 (or plasma density), ν and L. We determine L by setting it equal to the length over which the standing wave power is greater than the threshold power, as indicated schematically in Figure 1. In the thin approximation, this is given by

$$\begin{aligned} 4\ P_o \cos\ (k_o L_o) &= P_T \\ &= 1.44\ MW/cm^2\ P_r^2 \end{aligned} \tag{3}$$

where P_o is the incident power, P_T is the breakdown threshold in air, and P_r is the pressure in atmospheres. If we are well above threshold, the thin approximation breaks down and a numerical solution must be resorted to.

2.2 PLASMA FORMATION

The continuity equation is

$$\frac{dn_e}{dt} = n_e \left[A_i - A_{A2} - A_{A3} - A_D \right] \tag{4}$$

where A_i is the ionization rate, $A_{A2}(A_{A3})$ is the 2 body (3 body) attachment rate and A_D is the diffusion loss rate. The energy equation is

$$3/2\ d/dt\ n_e T_e = n_e \left[Q_J - Q_v - Q_x - \langle \varepsilon A_i \rangle - \langle \varepsilon A_D \rangle \right] \tag{5}$$

where Q_J is the power absorbed per electron, Q_v and Q_x are the rate of energy transfer to vibrational levels and electronic levels, respectively, and $\langle \varepsilon A_i \rangle$ and $\langle \varepsilon A_D \rangle$ is the rate of energy loss to ionization and diffusion, respectively.

We can write

$$n_e Q_J = f\ P_o \tag{6}$$

For small absorption, f is proportional to n_e, and thus Q_J is only a function of power. Solving these equations numerically, we find that the temperature quickly reaches a steady state, given by

$$T_e \left[A_i - A_2 - A_3 - A_D \right] = Q_J - Q_u - Q_x - \langle \varepsilon A_i \rangle - \langle \varepsilon A_D \rangle \tag{7}$$

If this temperature is higher than the breakdown temperature, about 2.1eV, then the right hand side of Equation 4 is positive, and the density exponentiates.

As the density increases, eventually the absorption fraction is approximately 100%, and the temperature starts to decrease. When it reaches the breakdown temperature again, $dn_e/dt = 0$, and the plasma

reaches a steady state. This behavior is shown qualitatively in Figure 2.

The breakdown temperature as a function of $P_r L$ is shown in Figure 3 (from Kroll and Watson). The density reached in steady state is

$$n_e/n_c = \nu/\omega \quad \frac{1}{k_o L} \quad \frac{P_o(MW/cm^2)}{1.44\ P_r^{\ 2}} \tag{8}$$

where n_c is the plasma density and the collision frequency is

$$\nu = \frac{7 \times 10^{12}\ P_R\ T_e}{(T_e + 4.94)} \quad sec^{-1} \tag{9}$$

The steady state density is independent of microwave frequency, inversely proportional to P_r and depends on incident power both through P_o and L. Using

$T_e = 2.1$ eV, we obtain

$$n_e = 1.4 \times 10^{13} \quad \frac{P_o\ (MW/cm^2)}{L\ P_R} \tag{10}$$

2.3 RADIATION

The radiation energy is made up of two parts: Q_v and Q_x. Q_v is the rate of energy transfer to vibrational levels in O_2 and N_2 and rotational levels in O_2. The major contributor is vibrational energy loss to N_2:

$$Q_u \quad = 1.53 \times 10^{12} \quad \frac{P_R}{T_e^{\ 3/2}} \quad e^{-2.6\ T_e} \qquad (eV/cm^3\ sec) \tag{11}$$

Using $T_e = 2.1$ eV, the total radiated energy per area through this channel is

$$P_v = n_e \quad \langle Q_v \rangle \quad L \tag{12}$$

$$= .0134\ P_o \quad (MW/cm^2)$$

Therefore, about 1.3% of the initial power is radiated through this channel at a characteristic energy level of 2.6 eV.

Q_x is the rate of collisional excitation of electronic levels in O_2 and N_2. The major contribution comes from two lines in N_2 at about 6.7 and 11.2 eV. The radiation rate from these lines is

$$\langle Q_x \rangle = 4.6 \times 10^{11} P_R \quad (eV/cm^3 \text{ sec}) \tag{13}$$

The total radiated energy is

$$\begin{aligned} P_x &= n_e \langle Q_x \rangle L \\ &= 1.03 P_o \quad (MW/cm^3) \end{aligned} \tag{14}$$

This says, that within the approximation of Equation (10) essentially 100% of the radiation is in these two lines, with about 2/3 in the 6.7 eV line and 1/3 in the 11.2 eV line.

2.4 SHOCK FORMATION

In a one-dimensional system, the shock strength can be defined in terms of the energy deposited per particle, $\overline{\Delta E}$:

$$M_1^2 = \frac{\gamma-1}{2\gamma} - \frac{\gamma+1}{2\gamma} - \left(1 + \frac{\Delta\overline{E}}{E_o}\right)\left(1 - \frac{\gamma-1}{\gamma+1}\,\frac{M_1^2-1}{M_1\left(1+\frac{\Delta E}{E_o}\right)}\right)$$

Where γ is the specific heat of the atmosphere, and E_o is the initial thermal energy. A good approximation is

$$M = 1 + \frac{\gamma+1}{8\gamma}\,\frac{\Delta\overline{E}}{E_o} \tag{16}$$

$\Delta\overline{E}$ is made up of two parts: The energy deposited collisionally in the plasma, and the energy radiated. We have seen from the previous section that the radiated energy predominates. A calculation of the amount of radiated power absorbed by the atmosphere is thus required. This task is outside of the scope of the present report.

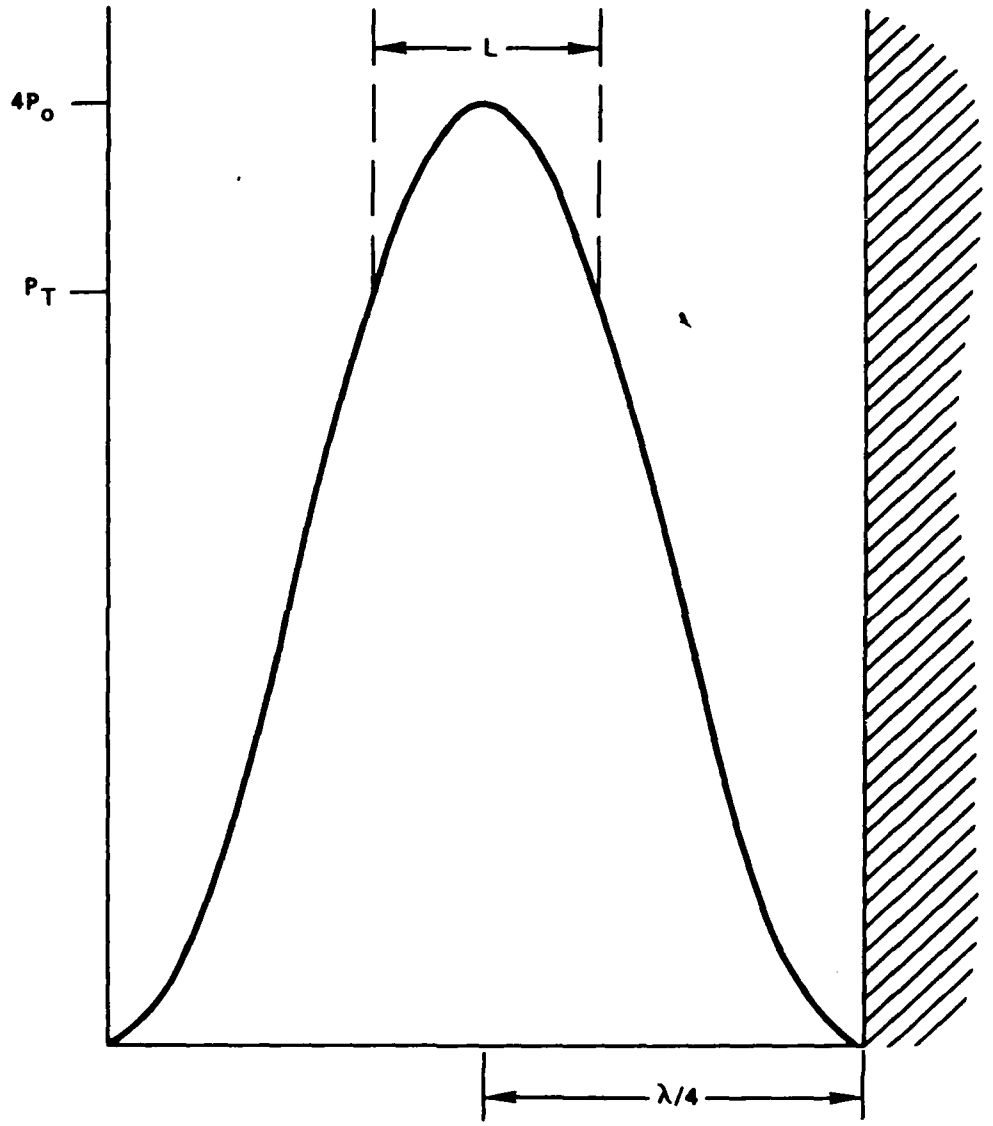

Figure 1. Geometry of breakdown model. Solid line is effective microwave density. Plasma is represented by uniform dielectric slab of width L.

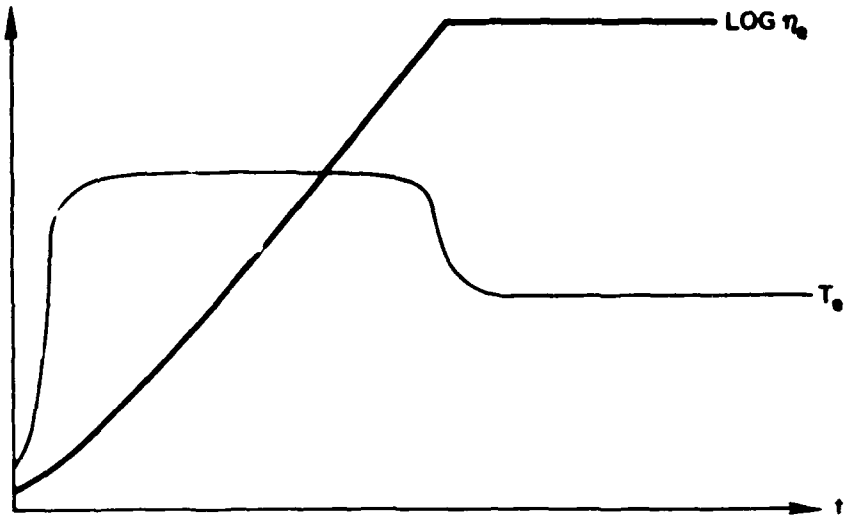

Figure 2. Characteristic time dependence of electron density and temperature during growth and saturation of breakdown.

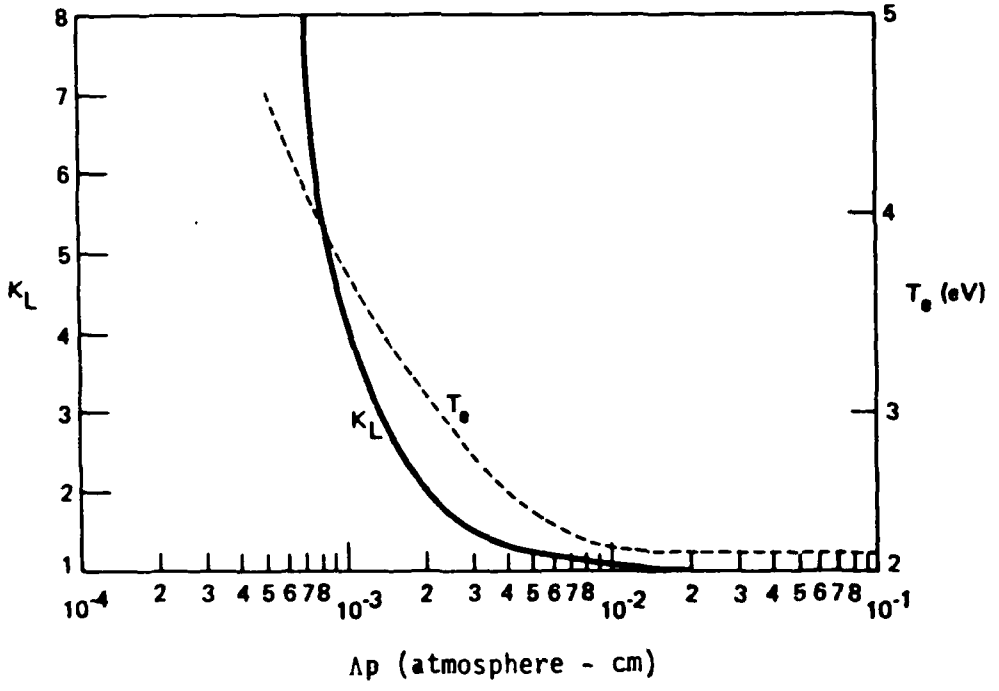

Figure 3. Electron temperature at breakdown threshold in air as a function of the product of pressure and diffusion scale length. Also shown is the function K_L, which represents the increase in breakdown threshold as a result of diffusion. When K_L = o, diffussion is negligible compared to attachment.

3.0 SUGGESTED EXPERIMENTS

Initial experiments should be directed toward testing and validation of breakdown theory in as simple an experimental configuration as possible. While waveguide and parallel plate configurations have been employed very successfully in the past for determination of breakdown thresholds, such configurations are unsuitable for the study of breakdown phenomenae at late times in the microwave pulse. It can be expected that ablation of material from the walls will strongly effect the atomic physics of the breakdown region. The experimental geometry then, should employ freely propagating, rather than guided, waves. As illustrated in Appendix C, the study and analysis of basic breakdwon phenomenae is greatly complicated by the presence of more than one breakdwon region, so the desired geometry should produce a standing electromagnetic wave pattern with only one antinode above breakdown threshold. This type of configuration can be obtained by focussing microwaves with a fast (f/3 or faster) lens onto a small target (about equal to, or somewhat smaller than, the focal spot diameter). The use of a small target increases the reflected wave divergence, reducing the standing wave intensity significantly at distances greater than about one target radius array. In experiments in this type of geometry, we were able to achieve power densities about 50% above threshold in the first standing wave maximum without exceeding threshold at other maxima. The major disadvantage of this configuration is the complexity of the electromagnetic wave pattern.

For comparison to theory, of particular interest is the parametric dependence of growth rate and saturation values of electron density and temperature, and of microwave absorption, on pressure, wavelength, and incident power. Experimental results, expressed in terms of normalized $p\Lambda$, ν/ω and P/P_T may be used to validate the scaling predictions of the breakdown model. The experimental apparatus described in Section 4 will enable variation of $p\Lambda$ by several orders of magnitude, from the diffusion dominated regime to a maximum value of approximately .1 atmosphere-cm, where attachment is strongly dominant. Similarly, ν/ω may be varied from as low as 10^{-4} to as high as about 35. The range of P/P_T would be limited by the characteristics of the standing wave pattern, as previously discussed.

The key parameters to be measured for comparison to theory are electron density and temperature and microwave absorption. Over the parameter range addressable with the apparatus described in Section 4, we expect electron densities in the range 10^{12} cm^{-3} to 10^{14} cm^{-3} and electron temperature of about 2 eV. With the exception of passive optical techniques, most standard plasma diagnostics appear to be unsuitable for application here. Probes severely perturb the breakdown phenomenae and must be looked on as highly suspect. While densities are in the typical range for millimeter wave interferometry, the small plasma size results in rather small phase shifts, making measurement difficult. Furthermore, due to the high pressure, the phase shift is determined by both plasma density and collisions, greatly complicating interpretation. The intense (close to 100% of the absorbed microwave power) optical and uV emission from the breakdown region makes optical observation the natural diagnostic, the only outstanding problem being interpretation of emission in terms of electron density and temperature. The approach taken in the IR&D work described in Appendix C, and recommended for future work, is to bypass the problem of interpretation of emission in terms of basic parameters, and instead compare observed and predicted intensities. In future work, intensity of specific observable lines, as well as total intensity, should be computed by the breakdown code. In addition, absolute intensities should be measured in experiments.

For measurement of microwave absorption, the techniques described in Appendix C appear suitable with modest improvements. An array of microwave receivers for the measurement of power reflected from the target region would be desirable.

Following experiments with a single breakdown region, the more realistic case of multiple breakdown regions would be in order. As illustrated in Appendix C, the breakdown region of maximum microwave absorption is not constant in time. A diagnostic capable of temporally resolving light emission from a number of regions simultaneously would be an asset. The framing camera and an array of photodiodes are two easily implemented candidates.

For shock wave generation measurements, one or more fast piezoelectric transducers may be mounted through the back of target, with the sensing

head flush with the target surface. One microsecond risetime transducer with sufficient sensitivity for measurements at pressures as low as a few mm Hg are available. Samples of data obtained using this technique can be found in Appendix C. Shadowgraph, Schlieren photography and/or holographic interferometry may also be utilized to study shock formation and propagation

Other phenomenae worthy of continued study, but outside the scope of this report, are filamentary structures in the breakdown region, which may occur both parallel and perpendicular to the target surface, and arc-like structures associated with surface irregularities in the target.

4.0 EXPERIMENTAL APPARATUS

The basic experimental apparatus is essentially the apparatus used in the IR&D microwave breakdown program, described in Appendix C. The 80 cm diameter, 120 cm long pressure vessel is of sufficient size to allow free space propagation for microwaves of wavelength smaller than about 6 cm, which was the largest wavelength considered. The chamber may be evacuated and backfilled with any desired gas. For most experiments, evacuation to about .01 torr by a rotary vane pump before filling is sufficient, though provision may be made for evacuation to 10^{-6} torr by diffusion pump for low pressure high purity experiments. For modest average power experiments, it does not appear necessary to continuously replace the target gas. We found excellent breakdown reproducibility running at 50 watt average power for periods of 20 minutes without replacing the fill gas. Wherever possible, internal chamber surfaces should be lined with microwave absorber. For low average power experiments, conventional pyrimidal foam absorbers (such as Emerson and Cummings CV type) are quite suitable. We have found that local heating and destruction of such absorber materials can become a problem at average input power levels of greater than about 200 watts. At higher power levels, an absorber more amenable to forced cooling (such as Emerson and Cummings FGM type) should be employed.

Horn fed reflectors, dielectric lenses and metallic delay lenses were considered for focussing antennae. The focal spot size and side lobe losses of these antennae are not greatly different for the same aperture size, so that choice of antenna may be based on other considerations, such as ease of construction and bandwidth. Reflectors are somewhat less suitable than lenses for focussing applications, as the location of the feed presents a problem. In a center fed reflector geometry, the feed may severely perturb the antenna pattern, while off-axis feed configurations tend to produce skewed radiation patterns. Construction is generally simpler for dielectric lenses than for metal plate lenses at wavelengths less than about 3 cm, while the reverse is true for longer wavelengths.

The maximum power density achievable with a focussing antenna of diameter D, and focal plane distance F, may be estimated from the expression for the intensity of the Fraunhoffer diffraction pattern of a circular aperture.

$$I = \frac{\pi}{4f^2} \frac{P}{\lambda^2} \left(\frac{2J_1(r)}{r} \right)^2 \qquad (1)$$

where J_1 is the first order Bessel function of the first kind, P is the total radiated power and f = D/F.

Real antenna patterns with main lobe radial intensity dependence very close to that given by (1) are easily obtained, but side lobe power is typically somewhat higher. In addition, some fraction of the microwave source power is lost in transmission and antenna mismatch. In order to minimize waveguide transmission losses, the source should be located as close as possible to the antenna feed, a factor which favors horn fed lenses over reflectors. With a moderate amount of care, focal spot intensities of about 80% of that given by (1), with P as the total microwave source power, should be achieved.

Typical high power microwave sources available commercially in the frequency range 6 to 35 GHz are shown in Table 1. Also shown are the maximum achievable power densities, and maximum air pressure for breakdown upon reflection from a conducting surface. In calculating the breakdown levels, a threshold of one quarter the free space value was assumed. It is worth noting, with reference to Table 1, that the maximum focal spot intensity achievable with typical commercial sources is nearly independent of frequency from 5.8 GHz to 35 GHz. The most powerful sources at 9.4 GHz and above are magnetrons, which are efficient and require relatively simple modulator systems. We have also shown a Crossed-Field Amplifier available at 9.4 GHz, as it is possible, if desired, to phase-coherently combine the outputs of several tubes to obtain higher power. The 5.8 GHz Twystron and Klystron amplifiers require considerable higher power and more complex modulators than the magnetrons. While experiments at several different frequencies are desirable in order to validate theoretical predictions of frequency scaling, the slight increase in experimental frequency range afforded by the use of a 5.8 GHz source does not justify the additional cost. The 9.4 GHz, 17 GHz, and 35 GHz tubes shown in Table 1 all have relatively modest pulse power input requirements, the highest being 34 kV

at 100 ampere for SFD303. A universal hard tube modulator, using for example an Eimac 4CW50,000E as a switch tube, capable of driving each of these tubes could be designed and fabricated at modest cost. The use of a hard tube modulator, rather than a Pulse Forming Network based system, would allow continuous variation from sub-microsecond to tens-of-microseconds pulse width, a very desirable feature for basic breakdown physics studies.

In the initial stages of the breakdown process, the electron density exponentiates from the ambient level, due to for example, cosmic radiation. In order to obtain a high degree of shot to shot reproducibility of the breakdown process in the laboratory, it is necessary to supply a reproducible "seed" density of electrons in the breakdown region. In our experiments, a 2 mA dc glow discharge, maintained by a biased (2kV) electrode located about 30 cm from the target region, was sufficient to reduce the breakdown jitter time from about 2 microseconds to about 50 nanoseconds, which was about the jitter in the microwave system.

f(GHz)	λ(cm)	P(kw)	TUBE NUMBER AND TYPE	MANUFACTURER	I_{max}(kW/cm^2)[1]	P_{max}(atm.)[2]
5.8	5.2	5000	VA146 TWYSTRON	VARIAN	116	.57
		5000	TH2067 KLYSTRON	THOMSON-CSF	116	.57
9.5	3.2	1500	SFD303 Mag.	VARIAN	92	.51
		1000	SFD233 CFA	VARIAN	61	.41
17	1.76	400	VF20 Mag.	FERRANTI	81	.47
35	.86	150	SFD327 Mag.	VARIAN	128	.60

TABLE 1

1. I_{max} is taken as 80% of the diffraction limited intensity with an f/1 antenna; i.e. $I_{max} = .8\pi P/4\lambda^2$.
2. P_{max} is taken as twice the free space value $p = (I/1440)^{1/2}$, where I is in kW/cm^2.

APPENDIX A
BREAKDOWN MODEL

In this appendix, we describe the calculation of absorption fraction and the solution of the density and temperature evolution equations.

Figure A1 shows a simple model of a plasma located at the first maximum of the standing wave pattern. We treat it as a *uniform material* of dielectric function

$$\epsilon = 1 - \frac{\omega_p^2}{\omega(\omega+i\nu)} \tag{1}$$

where ω_p is the plasma frequency, ω the microwave frequency, and the ν collision frequency. We solve the wave equation for the field amplitudes in 3 regions: 1) to the left of the plasma, 2) inside the plasma, and 3) between the plasma and the conducting plate. We take the origin to be at the center of the plasma. In region 1:

$$E_1 = e^{ik_oZ} + r_1 e^{-ik_oZ} \tag{2}$$

In region (2)

$$E_2 = t_1 e^{i\sqrt{\epsilon}k_oZ} + r_2 e^{-i\sqrt{\epsilon}k_oZ} \tag{3}$$

In region (3)

$$E_3 = t_2\left(e^{ik_oZ} + e^{-ik_oZ}\right) \tag{4}$$

Equation (4) satisfies the boundary condition at the conducting plate. Applying the proper boundary conditions at the plasma-vacuum interfaces, a short calculation gives the reflectivity, R, and the total absorption F = 1-R:

$$F = \frac{4\mathrm{Im}(AB^*)}{|A^2| + |B^2| + 2\mathrm{Im}(AB^*)} \tag{5}$$

where

$$A = \sin\phi\sin 2\sqrt{\varepsilon}\phi - \sqrt{\varepsilon}\cos\phi\cos 2\sqrt{\varepsilon}\phi$$

$$B = \sqrt{\varepsilon}\,\sin\phi\cos 2\sqrt{\varepsilon}\phi + \varepsilon\cos\phi\sin 2\sqrt{\varepsilon}\phi$$

$$\phi = k_o L/2$$

For small absorption and a thin breakdown region, $\phi \ll 1$, $\sqrt{\varepsilon}\phi \ll 1$, Equation (5) reduces to

$$F \approx 4(\mathrm{Im}\varepsilon)k_o L \tag{6}$$

This is the usual result, except for the factor 4 which results from the standing wave enhancement.

As the collision frequency increases, the absorption fraction increases, reaching a maximum at $\nu/\omega \sim 1$. Increasing the plasma density also increases the absorption; however, there is a maximum value, after which the wave is primarily reflected rather than absorbed. This behavior is shown in Figure (2). Appendix B explicitly evaluates F in terms of the real and imaginary parts of $\sqrt{\varepsilon}$.

The continuity and energy equations are:

$$\frac{dn_e}{dt} = n_e \left[\langle A_{io}\rangle + \langle A_{in}\rangle - \langle A_{A2}\rangle - \langle A_{A3}\rangle - \langle A_D\rangle\right] \tag{7}$$

$$\frac{3}{2}\frac{dn_e T_e}{dt} = n_e \left[\langle Q_J\rangle - \langle Q_V\rangle - \langle Q_X\rangle - \langle \varepsilon A_{io}\rangle - \langle \varepsilon A_{in}\rangle - \langle \varepsilon A_D\rangle\right] \tag{8}$$

The brackets $\langle\cdots\rangle$ refer to a Maxwellian average:

$$\langle \delta \rangle = \frac{2}{\sqrt{\pi} T_e^{3/2}} \int_0^{\infty} \sqrt{\epsilon}\, f e^{-\epsilon/T_e}\, d\epsilon \qquad (9)$$

We will discuss each of the rate constants and their average below.

A detailed theoretical investigation of cascade ionization of air by rf fields and laser beams was published by Kroll and Watson[1]. They solved the Boltzmann equation for the detailed distribution function $F(\epsilon,t)$. We will use the rate constants given by them, but assume that the distribution function is a Maxwellian. Kroll and Watson considered this approximation and found that ionization rates were different by a factor of approximately 2 from the Boltzmann calculation. This error is about the uncertainty in the rate constants. For this reason, and also since we are interested in the approach to steady state, when the plasma is sufficiently dense that the electron-electron collision time is shorter than the time scale of interest ($\sim$ 1μsec), we have used the simpler Maxwellian approximation.

A_{io} is the oxygen ionization rate. Ref.(1) gives it as

$$\begin{aligned} A_{io} &= 0 \qquad \epsilon < 12.06 \\ &= 1.3\times10^{9}\, P_R \sqrt{\epsilon}\, (\epsilon-12.06)\left[1 + .07(\epsilon-12.06\right] \quad \epsilon>12.06 \end{aligned} \qquad (10)$$

Here P_R is the pressure in atmospheres.

Averaging,

$$\langle A_{io} \rangle = 1.47\times10^{9}\, P_r T_e^{1/2} \left[12.06 + 3.68T_e + .42\, T_e^2 \right] e^{-12.06/T_e} \qquad (11)$$

A_{in} is the nitrogen ionization rate:

$$\begin{aligned} A_{in} &= 0 \qquad \epsilon<15.6 \\ &= 9.6\times10^{9}\, P_R \sqrt{\epsilon}\, (\epsilon-15.6)\left[1 + .05(\epsilon-15.6) \right] \quad \epsilon>156 \end{aligned} \qquad (12)$$

Averaging,

$$\langle A_{in} \rangle = 1.08 \times 10^{10} P_R T_e^{1/2} \left[15.6 + 3.56T_e + .3T_e^2\right] e^{-15.6/T_e} \quad (13)$$

A_{A2} is the two-body attachment rate due to the reaction $e + O_2 \rightarrow O^- + O$.

$$A_{A2} = 8.6 \times 10^8 P_R \sqrt{\varepsilon} \left[1.55/(\varepsilon+1)\right](\varepsilon-3.7) \quad e^{-.8(\varepsilon-6.7)^2} \quad (14)$$

A simple approximation which gives good results is to notice that A_{A2} is essentially a gaussian centered about 6.7eV.

Using this approximation, we find

$$\langle A_{A2} \rangle \cong 6.3 \times 10^9 \frac{P_R}{T_e^{3/2}} e^{-6.7/T_e} \quad (15)$$

A_{A3} is the three body attachment rate from the reaction $e+O_2+O_2 \rightarrow O_2^- + O_2$. It is

$$A_{AB} = 4.3 \times 10^7 P_R^2 \varepsilon \left[(1+.3\varepsilon)(\varepsilon+.08)^2\right]^{-1} \quad (16)$$

giving approximately

$$\langle A_{A3} \rangle = 2.3 \times 10^8 P_R^2 / T_e^{3/2} \quad (17)$$

except for very high pressures ($P_R >> 1$), $\langle A_{A2} \rangle$ is greater than $\langle A_{A3} \rangle$, in the temperature ranges of interest in our experiment.

A_D is the rate of loss of electrons due to diffusion. Defining the fusion scale length

$$\lambda = \left(ne / \frac{d^2 n_e}{dX^2}\right)^{1/2} \quad (18)$$

we have

$$A_D = \frac{2\varepsilon}{3m\nu_c \lambda^2} \quad (19)$$

Ref. (4) gives the electron-neutral collision rate as

$$\gamma_c = 7\times10^{12} \frac{(\varepsilon+.1)}{(\varepsilon+4.94)} P_R \tag{20}$$

Equation (19) describes free-electron diffusion. If the density is greater than $10^6/\lambda^2$, the ambipolar diffusion expression should be used, which means replacing λ by $\sqrt{m_e/m_i}\,\lambda \approx 36\lambda$. Thus

$$<A_D> = 3.6(1+T_e/5)/P_R\lambda^2 \tag{21}$$

Here we have taken $\lambda \approx L/2$.

We assume that the plasma size, L, is given by the distance between points where the standing wave power is greater than the threshold power: $4P_o \cos(2k_oL/2) = P_T$, giving $k_oL = \cos^{-1} P_T/4P_o$. We then allow the plasma to expand at the rate of $dL/dt = <A_D>$.

The power absorbed per electron is Q_J:

$$Q_J = F\, I_o/n_eL \tag{22}$$

where I_o is the microwave intensity in kw/cm^2. In calculating F, we take

$$<\nu_c> = 7\times10^{12} \frac{T_e}{Te+4.94} P_R \tag{23}$$

Q_v is the rate of energy transfer to vibrational levels in O_2 and N_2 and rotational levels in O_2. The major contributer to this term is vibrational energy loss to N_2:

$$\begin{aligned} Q_v &= Q_o+Q_n+Q_R \\ &\simeq Q_n \\ &= 6.0\times10^4\, P_R\sqrt{\varepsilon}\, e^{-4(\varepsilon-2.6)^2} \end{aligned} \tag{24}$$

Averaging, we find that a good approximation is

$$\langle Q_v \rangle = 1.53 \times 10^{12} P_R e^{-2.6/T_e} / T_e^{3/2} \quad (25)$$

Q_x is the rate of collisional excitation of electronic levels in O_2 and N_2. Kroll and Watson fit experimental data for the excitation rate constant A_x for three levels each of N_2 and O_2, using a simple analytical expression:

$$A_x = 0 \qquad \varepsilon < \beta$$

$$= \alpha \; P_R \sqrt{\varepsilon} \; (\varepsilon - \beta) e^{-\varepsilon/\gamma} \qquad \varepsilon < \beta$$

The various α, β and γ's are given in Reference 1. Averaging,

$$\langle Q_x \rangle = \sum_n \langle \varepsilon A_{xn} \rangle \quad (26)$$

$$= .88 P_R / T_e^{3/2} \sum_n \alpha_n / e^{-\alpha_n} / \delta_n \; \delta_R^2 \left(\beta_n^2 + 4 \beta_n \delta_n + 6 \delta_n^2 \right)$$

where $\frac{1}{\delta_n} = \left(\frac{1}{\beta_n} + \frac{1}{T_e} \right)$

The remaining terms in Equation (8) are energy loss due to ionization and diffusion. We simply model this by multiplying the averaged particle loss rate by the appropriate energy:

$$\langle \varepsilon A_{io} \rangle + \langle {}_{\varepsilon} A_{in} \rangle = 12.02 \langle A_{io} \rangle + 15.6 \langle A_{in} \rangle \quad (27)$$

$$\langle \varepsilon A_D \rangle = 3/2 T_e \langle A_D \rangle \quad (28)$$

Ionization threshold occurs when the right side of the continuity equation is zero:

$$\langle A_{io} \rangle + \langle A_{in} \rangle = \langle A_{A2} \rangle + \langle A_{A3} \rangle + \langle A_D \rangle \quad (29)$$

This defines a temperature required for breakdown. For pressures less than or about equal to atmospheric, and on the high pressure side of the Paschen curve, the dominant term on the right hand side is $\langle A_{A2} \rangle$. The characteristic temperature for breakdown is about 2 eV. At this temperature,

both $<A_{io}>$ and $<A_{in}>$ contribute. The pressure independence holds for $P_r\lambda \gtrsim 10^{-2}$. Setting the left side of the temperature equation to zero, we find the power required for threshold:

$$<Q_J> = FI_o/n_eL \tag{30}$$

$$= <Q_v> + <Q_x> + <\epsilon A_{io}> + <\epsilon A_{in}> + <\epsilon A_D>$$

The dominant contribution to the right side of Equation (30) is $<Q_x>$, electronic excitations. For small absorption, we find, using (6):

$$Q_J = 4 \frac{1}{n_c} \frac{\nu}{1 + \nu^2/\omega^2} I_o/c \tag{31}$$

Evaluating Equation (30) using Equation (31) gives the breakdown threshold. Experiments show that

$$I_o = 1.44 \times 10^3 P_R^2 \quad kw/cm^2 \tag{32}$$

for $P_r\lambda$ greater than .01, where the diffusion term is small. Kroll and Watson have adjusted the coefficient of $<Q_x>$ in order to obtain agreement with Equation (32) in their kinetic treatment. Our Maxwellian treatment underestimates the breakdown level by about 50%.

We have solved Equations (7) and (8) numerically as a function of time. A typical set of results for temperature, density, absorption fraction and radiation are shown in Figure (3). In a very short time on the order of 10^{-10} sec, the temperature equilibrates at a value given by

$$Q_L(T_o) = <Q_J> = F \frac{I_o}{n_eL} \tag{33}$$

$$= 4 \frac{k_oL}{n_c} \frac{\omega}{\nu} \frac{I_o}{\left(1 + \frac{\omega^2}{\nu^2}\right) L}$$

Where Q_L is the sum of the energy loss rates. This equation is independent of n_e and L, and only depends on I_o and P_R. The density then exponentiates at a rate given by

$$n_e = n_o \exp \left[\langle A_i \rangle - \langle A_L \rangle \right] \tag{34}$$

where $\langle A_i \rangle$ is the sum of the ionization rates and $\langle A \rangle$ is the sum of the electron loss rates. The density continues to increase until $F \approx 1$. Now $\langle Q_J \rangle$ is no longer independent of n_e. The temperature begins to decrease until it reaches the threshold temperature T_T, at which time the density remains constant.

We may derive a simple expression for the steady state density. If $F \approx 1$, then

$$n_e = \frac{I_o}{Q_L L} \tag{35}$$

We may calculate $Q_L(T_T)$ by going back to the definition of breakdown threshold power:

$$F \frac{I_{oT}}{n_L} = Q_L(T_o, P_R)$$

Experimentally it is found that

$$I_{oT} = 1.44 \times 10^3 P_R^2 \text{ kw/cm}^2 \tag{36}$$

These experiments do not have the factor of 4 standing wave enhancement, so $F = \frac{n}{n_c} \omega/\nu \, k_o L$, giving

$$Q_L = \frac{1}{n_e} \frac{\omega}{\nu} k_o L \frac{I_{oT}}{L} \tag{37}$$

Substituting into Equation (35) we find

$$\frac{n_e}{n_c} = \nu/\omega \, k_o L \, \frac{I_o}{1.44 \times 10^3 \, P_R^2} \tag{38}$$

Since n_c is proportional to ω^2, Equation (38) is independent of microwave frequency. Since ν is proportional to P_R, n_e goes inversely with PR, and, of course is linear with I_o. If I_o is a constant fraction of the breakdown threshold in the ambient gas, $I_o = \alpha I_{oT}$, Equation (38) becomes

$$\frac{n_e}{n_c} = \nu/\omega \; \alpha/k_o L \tag{39}$$

and n_e is then proportional to P_R. The numerical model discussed agrees well with Equation (39), except that, as discussed above, the breakdown power is about 50% too low.

Reference

1. N. Kroll and K. M. Watson, "Theoretical Study of Ionization of Air by Intense Laser Pulses", Phys. Rev. A 5, 1883 (1972).

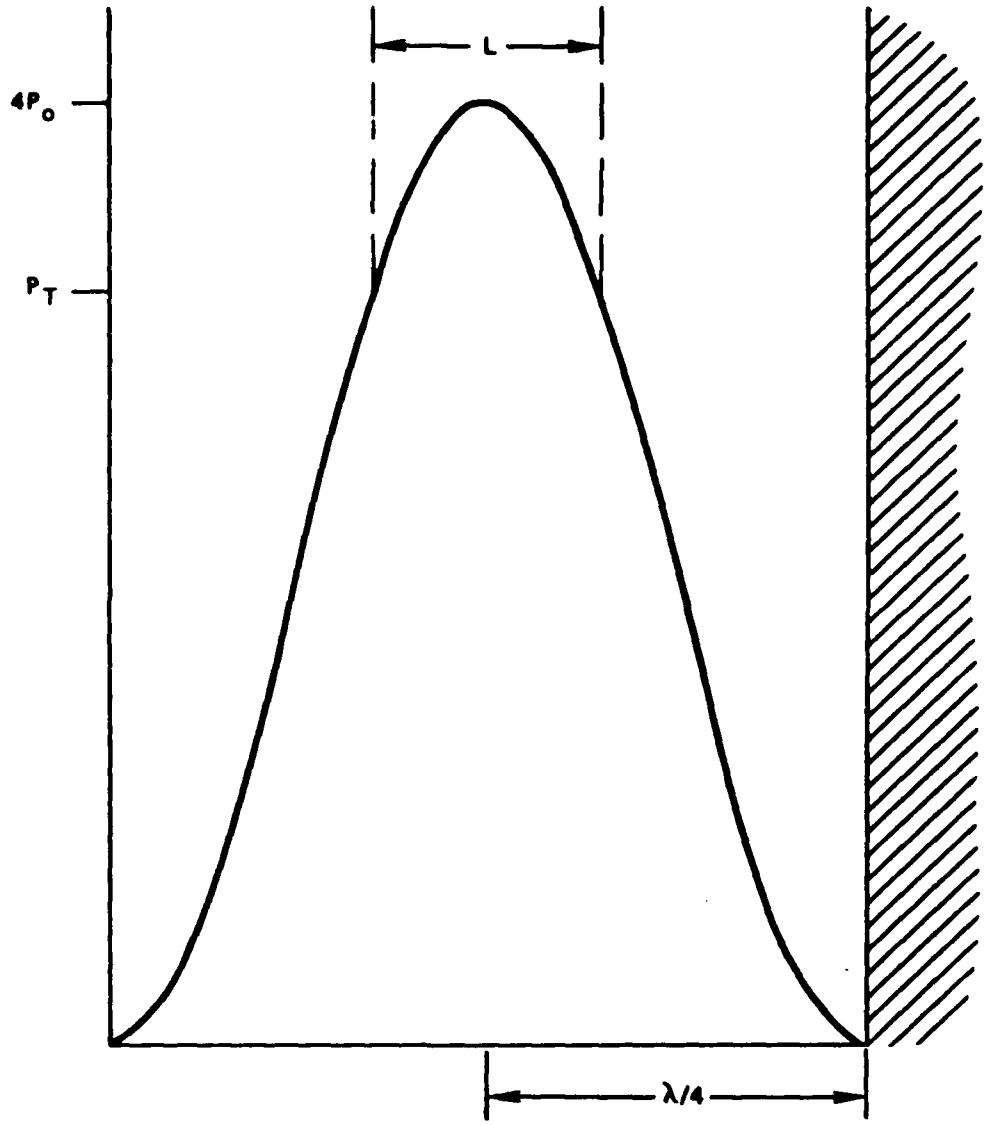

Figure A-1. Geometry of breakdown model. Solid line is effective microwave power density. Plasma is represented by uniform dielectric slab of width L.

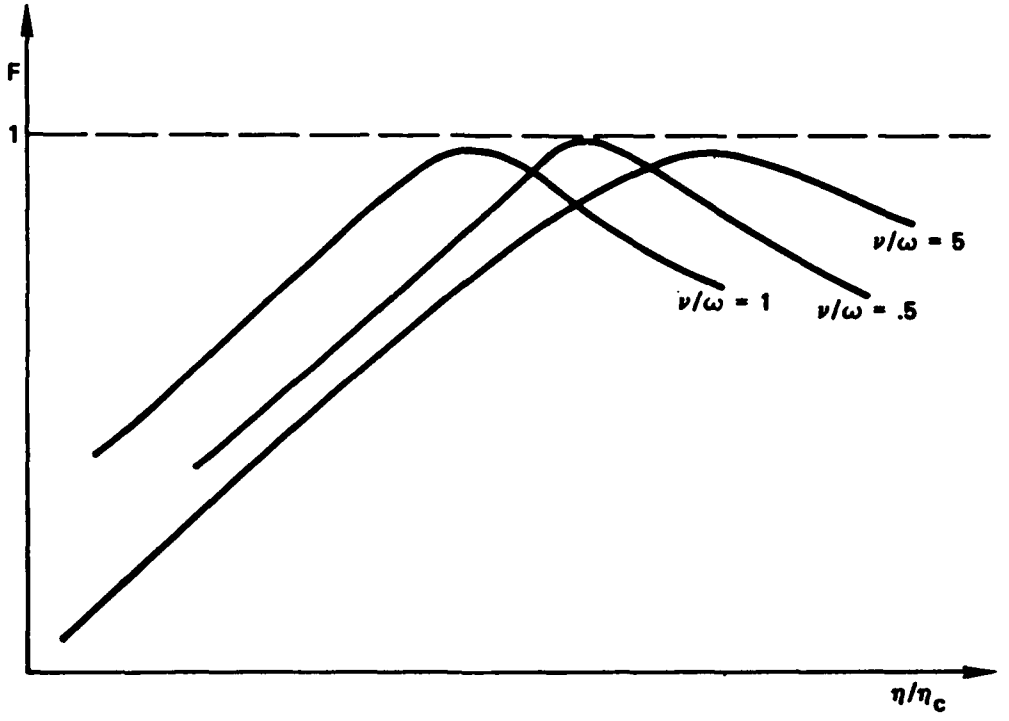

Figure A-2. Microwave absorption fraction as a function of electron density, with electron collision frequency as a parameter.

APPENDIX B
EVALUATION OF ABSORPTION

Evaluation of the absorption fraction. The dielectric function is

$$\varepsilon = 1 - \frac{\omega_p^2}{\omega^2\left(1 + \nu^2/\omega^2\right)} + i\,\frac{\omega_p^2\,\nu/\omega}{\omega^2\left(1 + \nu^2/\omega^2\right)} \tag{B1}$$

$$= \varepsilon_R + i\varepsilon_i$$

so that

$$\gamma \equiv R_e\,\sqrt{\varepsilon} = \left(\varepsilon_R^2 + \varepsilon_i^2\right)^{1/4} \cos\,(\theta/2) \tag{B2}$$

$$\delta \equiv Im\,\sqrt{\varepsilon} = \left(\varepsilon_R^2 + \varepsilon_i^2\right)^{1/4} \sin\,\left(0/2\right)$$

where

$$\theta = Tan^{-1}\left(\varepsilon_i/\varepsilon_R\right)$$

Define

$$\alpha = 2\phi\gamma$$

$$\beta = 2\phi\delta$$

then

$$\sin 2\sqrt{\varepsilon}\,\phi = \sin\alpha\,\cosh\,\beta + i\cos\alpha\,\sinh\,\beta$$

$$\sin 2\sqrt{\varepsilon}\,\phi = \cos\alpha\,\cosh\,\beta - i\sin\alpha\,\sinh\,\tilde{\beta}$$

then

$$A = a_r + ia_i$$

$$= \left[\sin\phi \sin\alpha \cosh \beta - \cos\phi \,(\gamma \cos\alpha \cosh \beta + \delta \sin\alpha \sinh \beta)\right] \tag{A3}$$

$$+ i\left[\sin\phi \cos\alpha \sinh \beta - \cos\phi(\delta \cos\alpha \cosh \beta - \gamma \sin\alpha \sinh \beta)\right]$$

Further define

$$b_r \equiv \sin\phi \cos\alpha \cosh \beta + \cos\phi(\gamma \sin\alpha \cosh \beta - \delta \cosh \beta) \tag{A4}$$

$$b_i \equiv -\sin\phi \sin\alpha \sinh \beta + \cos\phi(\gamma \cos\alpha \sinh \beta + \delta \sin\alpha \cosh \beta)$$

Then

$$B = (\gamma b_r - \delta b_i) + i\,(\delta b_r + \gamma b_i) \tag{A5}$$

Then

$$I_m\, AB^* = \gamma(a_i b_r - a_r b_i) - \delta\,(a_i b_i + a_r b_r)$$

$$|A^2| = a_r 2 + a_i{}^2 \tag{A6}$$

$$|B^2| = (\gamma b_r - \delta b_i)^2 + (\delta b_r + \gamma b_i)^2$$

which may be used to explicitly evaluate the absorption fraction

$$F = \frac{4\, I_m\, AB^*}{|A^2| + |B^2| + 2\, I_m\, AB^*} \tag{A7}$$

APPENDIX C

MICROWAVE BREAKDOWN EXPERIMENTS - TRW IR&D PROGRAM

1. INTRODUCTION

In 1980 and 1981, a series of experiments on microwave breakdown were conducted at TRW under an IR&D program. An existing laboratory facility was modified for the investigation of breakdown in front of a conducting surface. Initial experiments were designed to test some of the basic results of the theory presented in Appendices A and B, in particular, the growth and saturation of electron density in the breakdown region and absorption of the incident microwave power. Other phenomenae, not treated by the theory, such as the behavior of multiple breakdown regions, filamentation, and shock wave generation, were observed and investigated in varying detail.

The experimental apparatus is described in Section 2, and the results summarized in Section 3.

2. EXPERIMENTAL APPARATUS

The experimental configuration is shown schematically in Figure C-1. Microwave radiation at a frequency of 9.4 GHz was focussed to a spot size (FWHM) of approximately 6 cm by 12 cm onto a target inside the pressure vessel. The antenna was a rectangular horn-fed dielectric lens with a 18 cm by 31 cm aperture and an aperture to focal plane distance of 60 cm. The microwave source was a surplus Navy radar system utlizing a 4J50 magnetron with maximum peak power of 200 KWatt, modified for longer pulse widths and variable repetition rate. Available pulse widths varied from .5 to 7 microseconds, and repetition rate from single shot to 1000 pps. Most experiments were performed with the 7 microsecond pulse width and 10 pps typical. The 80 cm diameter by 120 cm long stainless steel pressure vessel was evacuated by rotary pump and diffusion pump to a base pressure of 10^{-6} torr and could be backfilled to any desired pressure with air, nitrogen, argon, helium, hydrogen or any mixture thereof. The conducting target was suspended in the focal plane region by a dielectric rod. A sliding vacuum feedthru enabled adjustment of the target position both parallel and perpendicular to the microwave beam propagation direction. The target material was aluminum or copper, and a variety of sizes were tested in order to modify the reflected wave pattern. Some target designs included integral diagnostics, such as a microwave receiver or piezoelectric pressure transducer.

A number of diagnostics were installed on the system at various times during the program. Visual and conventional photographic observation of the breakdown region was always possible through several windows on the chamber. Light from the breakdown region was focussed by f/5 optics onto the input slit of a .3 meter monochromator and detected with a photomultiplier tube. The photomultiplier signal was recorded either by an oscilloscope or a "boxcar" sampling instrument (PAR Model 162). A rotatable mirror in the optics system allowed spatial scanning of the breakdown region. A special target was used for the microwave absorption measurements. A sample of the microwave power incident on the target was coupled through a small hole in the center of the target to a crystal detector. A second crystal detector mounted on a microwave horn situated near the dielectric window (see Figure 1)

provided a measurement of power reflected from the target and breakdown region. For shock wave measurements, the target was constructed with a fast piezoelectric transducer mounted flush with the target surface. A number of attempts were made to measure local properties of the breakdown region (e.g., conductivity) and the local value of the microwave field strength near the breakdown region, using small probes. Though the data obtained in these measurements was not obviously spurious, it was clear from visual observations that the probes severely perturbed the breakdown region, and this line of investigation was discontinued.

During 1981, a second apparatus was constructed in order to test the use of shadowgraph and Schlieren photography as a diagnostic for breakdown at atmospheric pressure. Microwave fields sufficient to achieve breakdown at atmospheric pressure with the available 200 kWatt 9.4 GHz source were obtained in the modified open ended waveguide configuration shown in Figure C-2. The setup for shadowgraph production is shown schematically in Figure C-3. The Q-switched ruby laser produced 50 ns pulses at any desired time with respect to the microwave pulse.

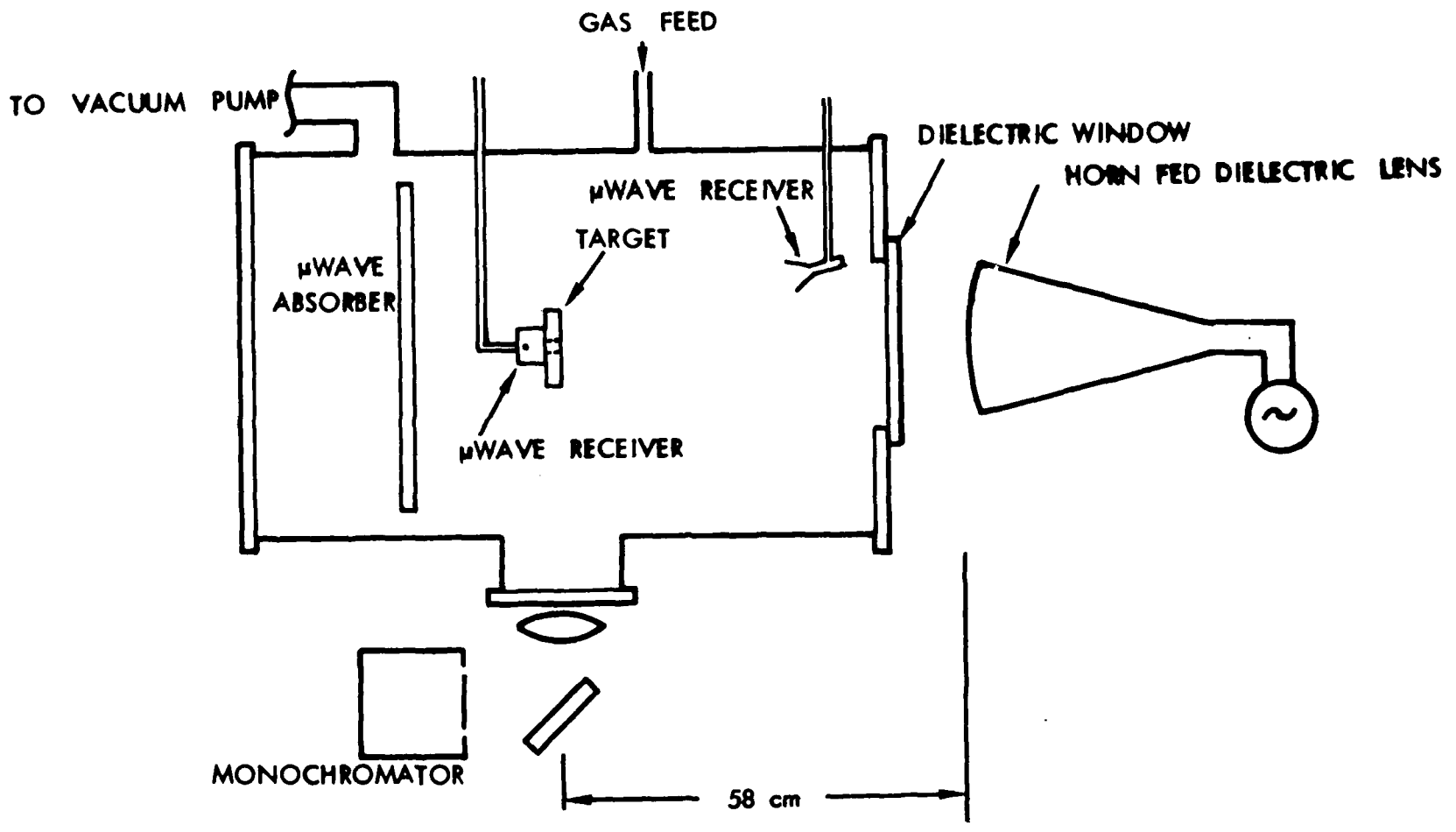

Figure C-1. Experimental apparatus for the study of microwave breakdown in front of a conducting surface.

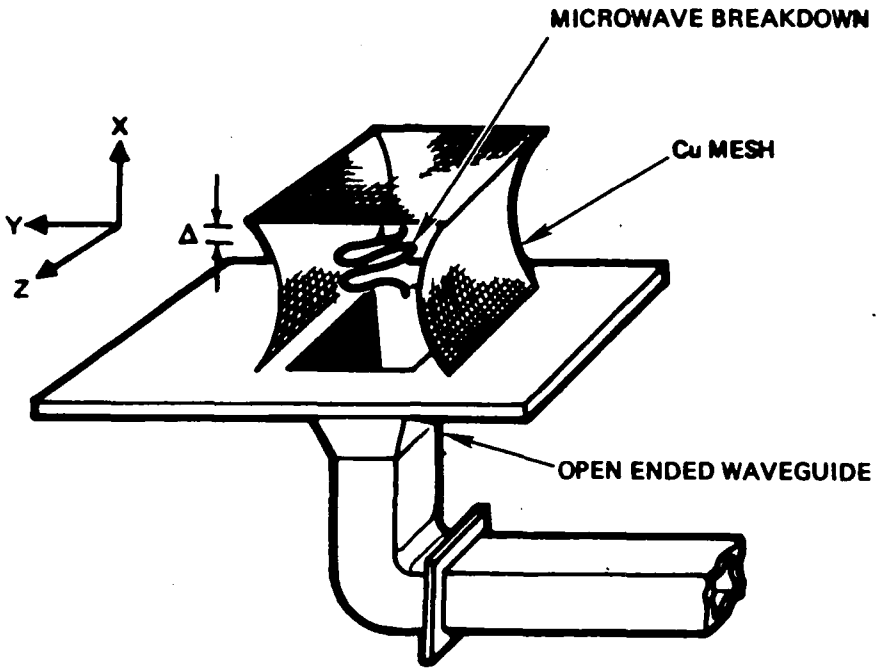

Figure C-2. Setup for microwave breakdown at atmospheric pressure in a waveguide like geometry.

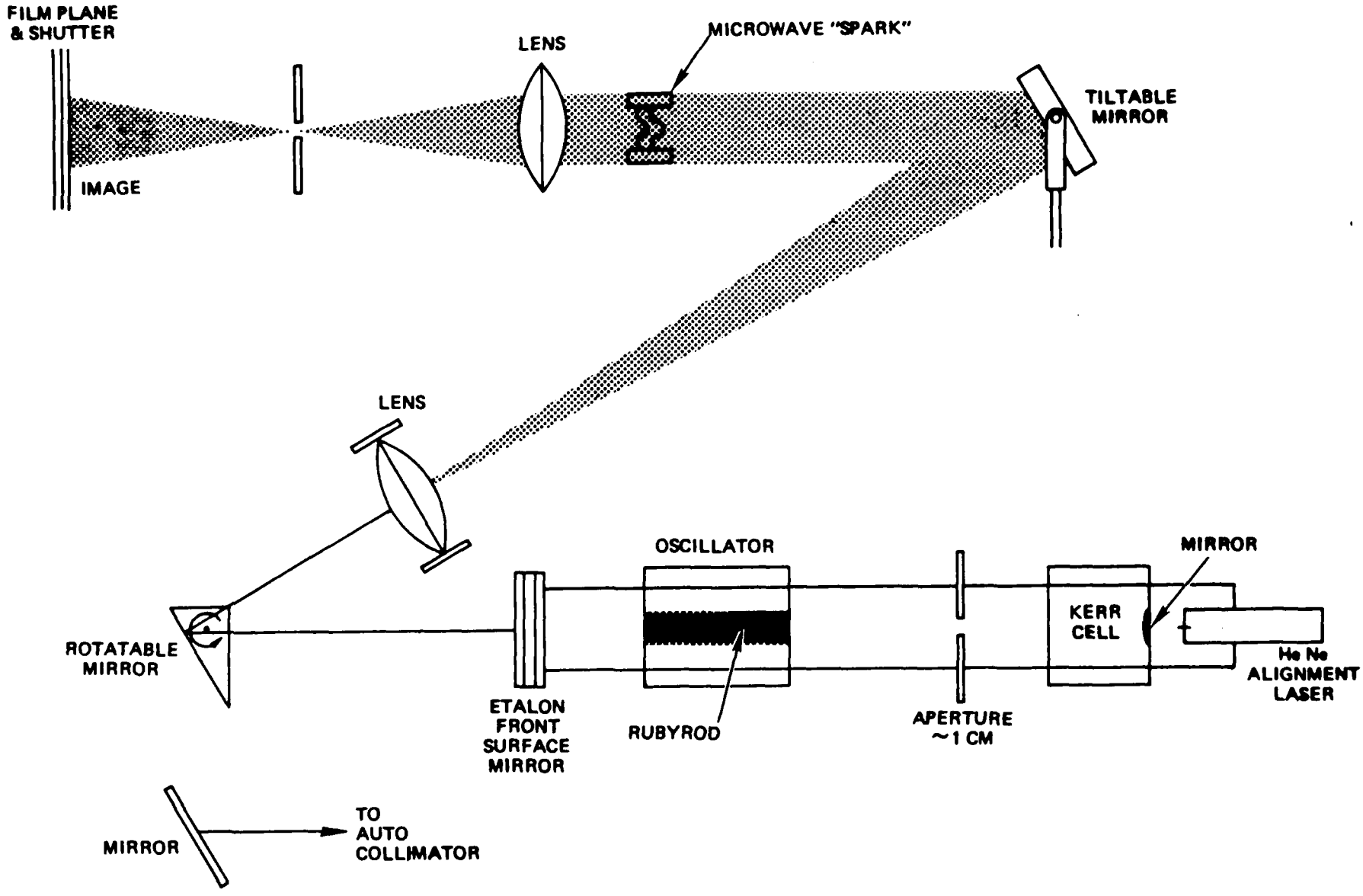

Figure C-3. Shadowgraph setup.

3. RESULTS

3.1 GROWTH AND SATURATION OF BREAKDOWN

The first series of experiments was designed to test the basic predictions of the analytic model described in Appendix A. Typical results obtained by numerical integration of the model equations are illustrated in Figure C-4, for an incident microwave intensity of 5 kW/cm^2 and an ambient air pressure of .1 atmosphere. The electron density rises from the initial value of $10^6 cm^{-3}$ to a saturated value of $10^{13} cm^{-3}$ in about one microsecond. Saturation occurs as a result of absorption of the microwave radation, which reaches a value close to one as the density saturates.

Excellent qualitative, and reasonable quantitative, agreement was found between the experimental results and the analytic model predictions. As expected, when the incident microwave intensity was between 25 and about 35 percent of the threshold for breakdown without a surface present, breakdown occurred only at the first peak of the standing wave pattern, 1/4 wavelength from the plate. The breakdown region was "pancake" shaped, with a thickness of approximately 3 mm. At higher ratios of incident to threshold power, breakdown occured at additional standing-wave peaks, greatly increasing the complexity of measurement and analysis. Discussion in this section is confined to the case of a single breakdown region. Some experimental results on multiple breakdown regions are described in Section 3.2.

As direct measurements of electron density and temperature were not avaiable, we compared instead the characteristic temporal behavior of the observed emitted light intensity with that predicted by the theoretical model. It should be noted that the intensity predicted by the theoretical model is actually due to ground state ultraviolet transitions, while the observations were made in the visible portion of the spectrum. However, the temporal behavior of all lines is expected to be nearly identical as long as the electron temperature variation is small compared to the upper state energy of the transition, an assumption which appears to be justified.

Figure C-5 shows the observed nitrogen second positive band head intensity during the first 2 μsec of the pulse, at a pressure of 29 mm Hg in air. Figure C-6 shows the analytic prediction for nitrogen line radiation under similar conditions, and exhibits the same characteristic exponential growth and rapid saturation as shown in the experimental data.

The analytic predictions of very high absorption in the breakdown region are also supported by experiment. Figure C-7(b) shows the microwave power reflected from the target region with (solid line) and without (dotted line) air breakdown, and indicates absorption of 75 to 90 percent of the incident microwave power by the breakdown region after the first microsecond of the pulse. A corroborative measurement of the absorption is illustrated in Figure C-7(c), which is a measurement of the fraction, T, of the incident power transmitted through the breakdown region. If the fraction of the incident power reflected by the breakdown region is small (as Figure C-7(b) would suggest), then the absorption fraction is $(1 - T^2)$. Thus, the data of Figure C-7(c) would indicate an absorption of 60 to 80 percent, in fairly good agreement with the reflected power measurement. It also should be noted, with reference to Figure C-7(a), that saturation of electron density, as indicated by saturation of light emission, in the breakdown region occurs when absorption becomes large, as predicted by the analytic model.

3.2 MULTIPLE BREAKDOWN REGIONS AND OTHER PHENOMENA

As the incident power was raised at fixed pressure, or the pressure reduced at fixed power, breakdown occured at additional standing wave peaks. As many as ten visually distinct breakdown regions were observed before breakdown became diffuse. The temporal dependence of light emission from a a single breakdown region, which is a good indicator of the microwave absorption in that region, was found to be a strong function of the number of individual breakdown regions occurring. Figures C-8 and C-9 illustrate the nitrogen second band head light emission from the first breakdown region at ambient air pressures from 31.6 mm Hg to 15.0 mm Hg, at fixed incident microwave power. For timing reference, Figure C-10 shows the incident microwave pulse along with the light emission at 27.0 mm Hg pressure. At 31.6 mm Hg, the highest pressure at which breakdown occurred reproducibly, light emission saturates about 4 microseconds into the pulse and remains constant until the incident power begins to drop. At lower pressures, light

emissions saturates earlier, due to the higher electron density growth rate. The peak light emission is nearly independent of pressure. However, as the pressure is lowered, and additional breakdown regions appear, the light emission late in the pulse drops significantly. At the lowest pressures shown, 15 to 17 mm Hg, the emission late in the pulse is less than one tenth the peak emission. Apparently, the incident microwave power is absorbed predominantly in the first breakdown region early in the pulse, but is absorbed more strongly in other regions later in time. This behavior is illustrated in Figure C-11, which shows light emission as a function of distance from the target at various times during the microwave pulse. In this case the fill gas was Helium at a pressure of approximately .5 atmosphere. Emission from the first region grows and saturates in the first microsecond of the pulse, at which time the emission from the second region is about 5% of that from the first region. The second breakdown region continues to develop in time, resulting in a reduction of the microwave field at the first region. At a time of 2 microseconds, the light emission from the second breakdown region exceeds that from the first. The details of the breakdown process for multiple breakdown regions are by no means understood at this time, and considerably more experimental and theoretical effort needs to be spent in this area.

All gases examined exhibited some degree of filamentation in the breakdown region. Filamentation was particularly strong in the case of Argon, where 100% fluctuations in emitted light and microwave absorption were observed, as illustrated in Figure C-12.

3.3 SHOCK WAVE GENERATION

Shock wave generation due to heating in the breakdown region was observed with a fast (1 μs rise time) piezoelectric transducer mounted flush with the target surface. At a fill pressure of .5 psi (29 mm Hg) of air, a peak overpressure of .075 psi, or 15%, was observed. The pressure wave consisted of a compression pulse with a duration of typically 8 μsec (FWHM), followed by a rarefraction pulse of somewhat smaller amplitude and larger duration (typically 20 μsec). When the microwave intensity was adjusted to obtain breakdown at several (up to 6) standing wave peaks, pressure pulses were detected from each breakdown region. Typical transducer output signals are shown in Figures C-13 and C-14, for air breakdown at a pressure of 25.3 mm Hg and Helium breakdown at a pressure of about .5 atmosphere respectively.

Since the breakdown region was shaped roughly like a disk of 5 cm diameter and .3 cm thick (measured optically), and the distance from the first breakdown region to the target was .8 cm, the shock propagation should be well described by a one dimensional approximation. The measured over-pressure of 15% then corresponds to a 30% increase in the neutral gas energy density in the breakdown region. Therefore, at the ambient air pressure of 29 mm Hg, using the measured breakdown region width of .3 cm, the total energy deposited in the form of neutral gas energy was approximately 2.5×10^{-3} joule/cm^2, which is about 25% of the incident microwave energy.

Of particular interest is the scaling with pressure of neutral gas heating and shock formation. We have developed some elementary models of scaling, and estimate that the fraction of incident microwave energy deposited in the neutral gas should be independent of gas pressure. Since the breakdown threshold increases as the square of the pressure, the neutral gas energy increase per molecule would then increase linearly with pressure. Scaling from our experimental results at 29 mm Hg air pressure, this simple model would predict a peak shock pressure of about about 5 atmospheres, corresponding to a Mach 2 shock, at an ambient pressure of one atmosphere. Unfortunately, with the experimental apparatus available, we were not able to operate over a sufficient pressure range to test the scaling estimates. Further experimental work with upgraded apparatus is highly recommended. The use of a slightly faster microwave lens and a commercially available higher power ($\sim$ 1.5 MWatt) microwave source at the same frequency would enable measurements at pressures up to at least .2 atmospheres in the same experimental configuration.

A diagnostic of shock formation and propagation would be a valuable addition to future experiments. Shadowgraph and/or Schlieren photography was identified as a potentially valuable diagnostic tool, and a separate experimental apparatus, already described in Section 2, was designed and constructed for preliminary tests. The microwave discharge proved to be sufficiently reproducible to allow study of the time development of the breakdown on a shot-to-shot basis. Shadowgraphs of the breakdown region at t = 0, .3, .6, 1.0 and 1.4 microseconds are shown in Figures C-15 and C-16. In this particular experiment, a wire (visible in the photographs) was inserted in the breakdown region to provide a high field region for initiation of the discharge. This technique will require further development, especially in the areas of recording and analysis, but appears to be a potentially powerful tool in the study of breakdown physics.

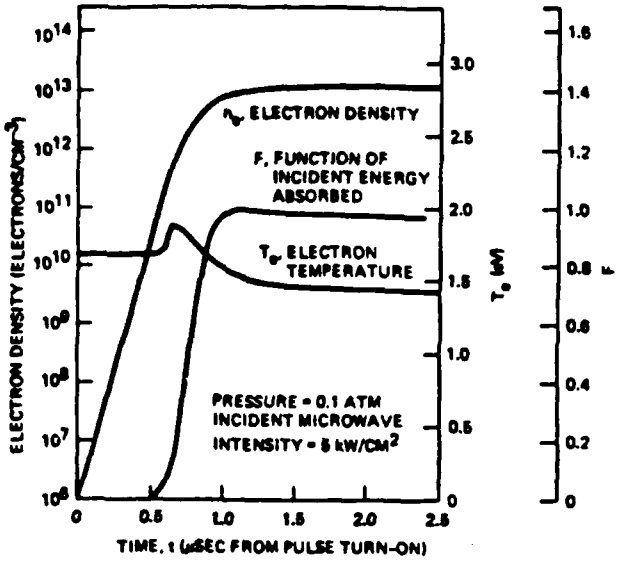

Figure C-4. Time history of electron density and temperature and microwave absorption fraction as predicted by the theoretical model described in Appendix A.

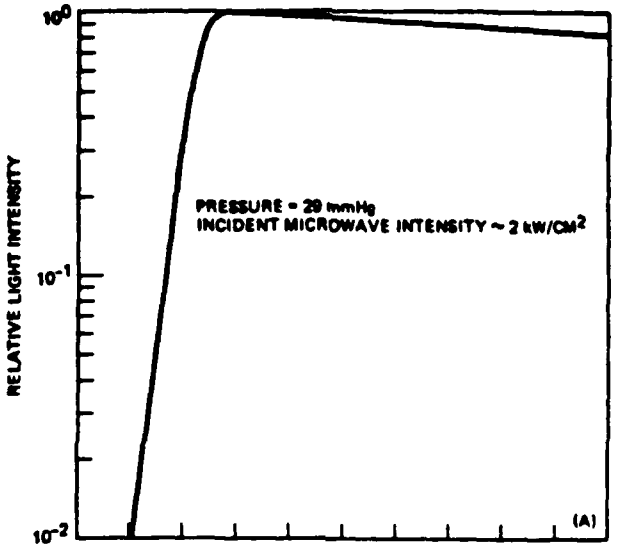

Figure C-5. Experimentally observed time history of Nitrogen 3577A line intensity in air breakdown at a pressure of 29 mmHg.

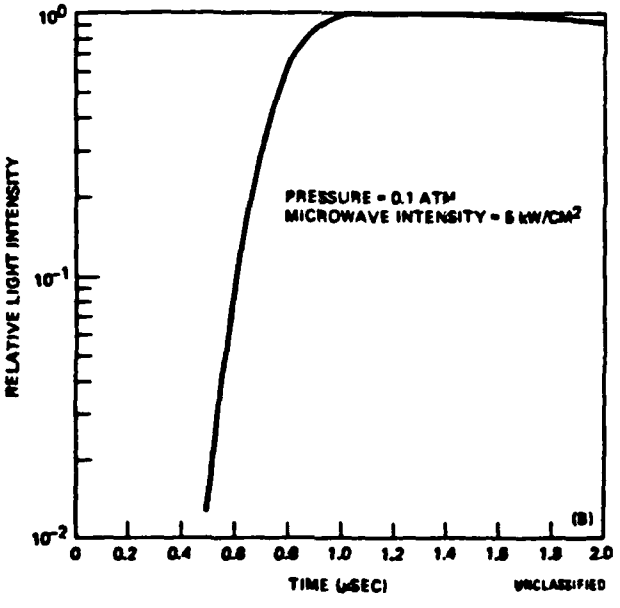

Figure C-6. Theoretically predicted total line emission in air breakdown at .1 atmosphere.

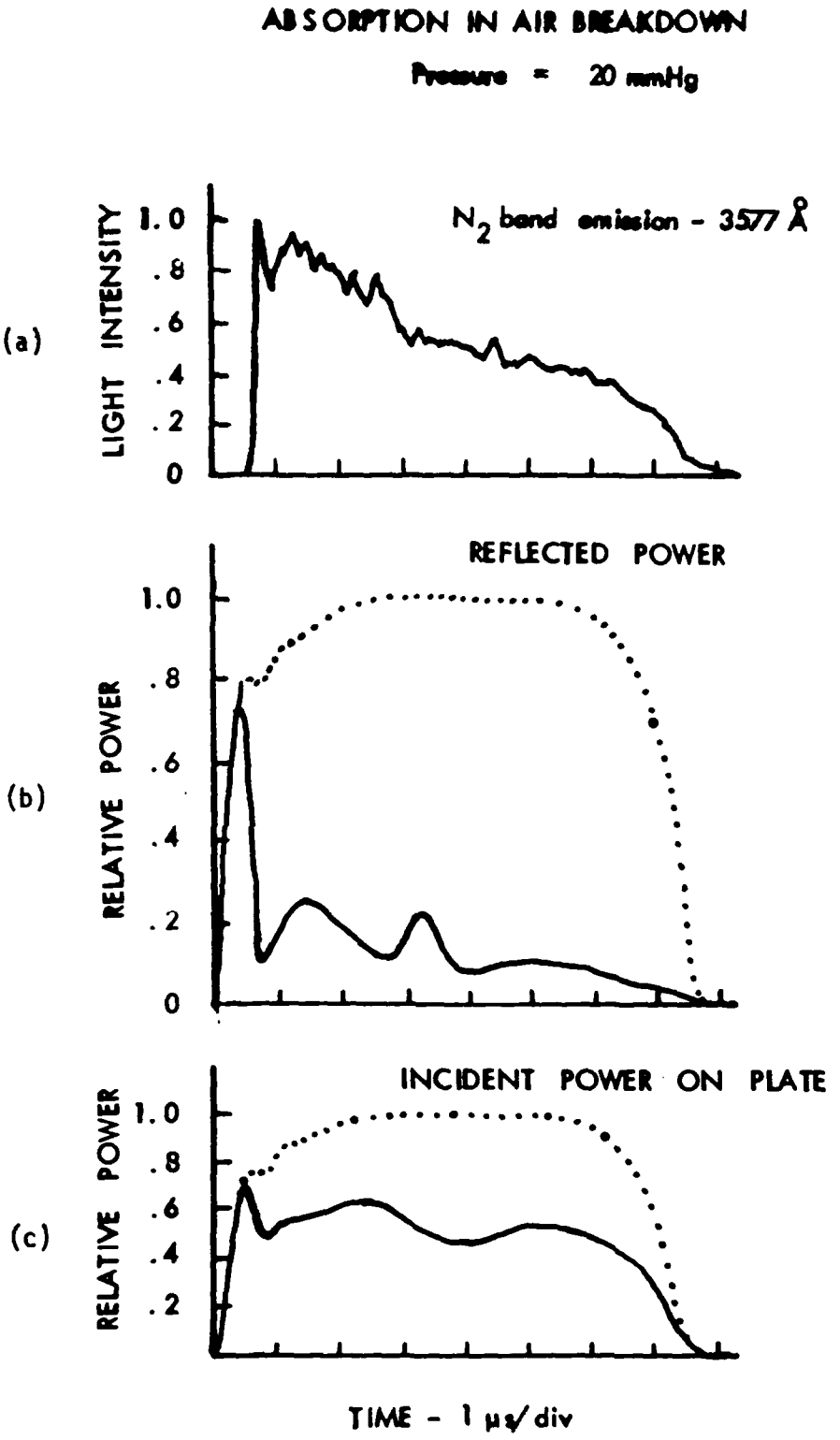

Figure C-7. Experimentally observed time history of (a) Nitrogen line emission from breakdown region; (b) microwave power reflected from target and; (c) microwave power incident on target. The dotted lines in (b) and (c) are received microwave power without breakdown, obtained by raising the gas pressure until no breakdown occurred.

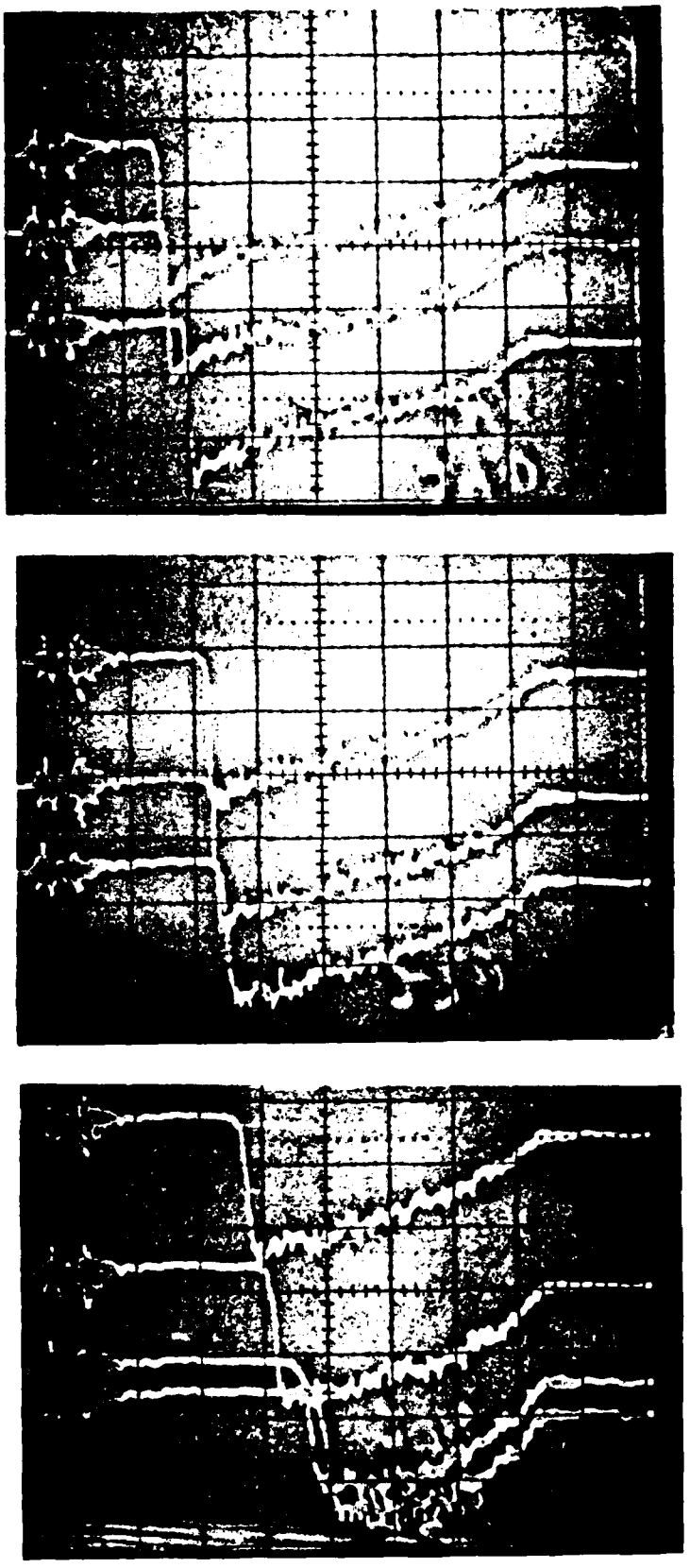

Figure C-8. Time history of 3577A line emission for air breakdown at pressures from 24.0 to 31.6 mmHg, fixed power. Horizontal scale is 1 μs/div.

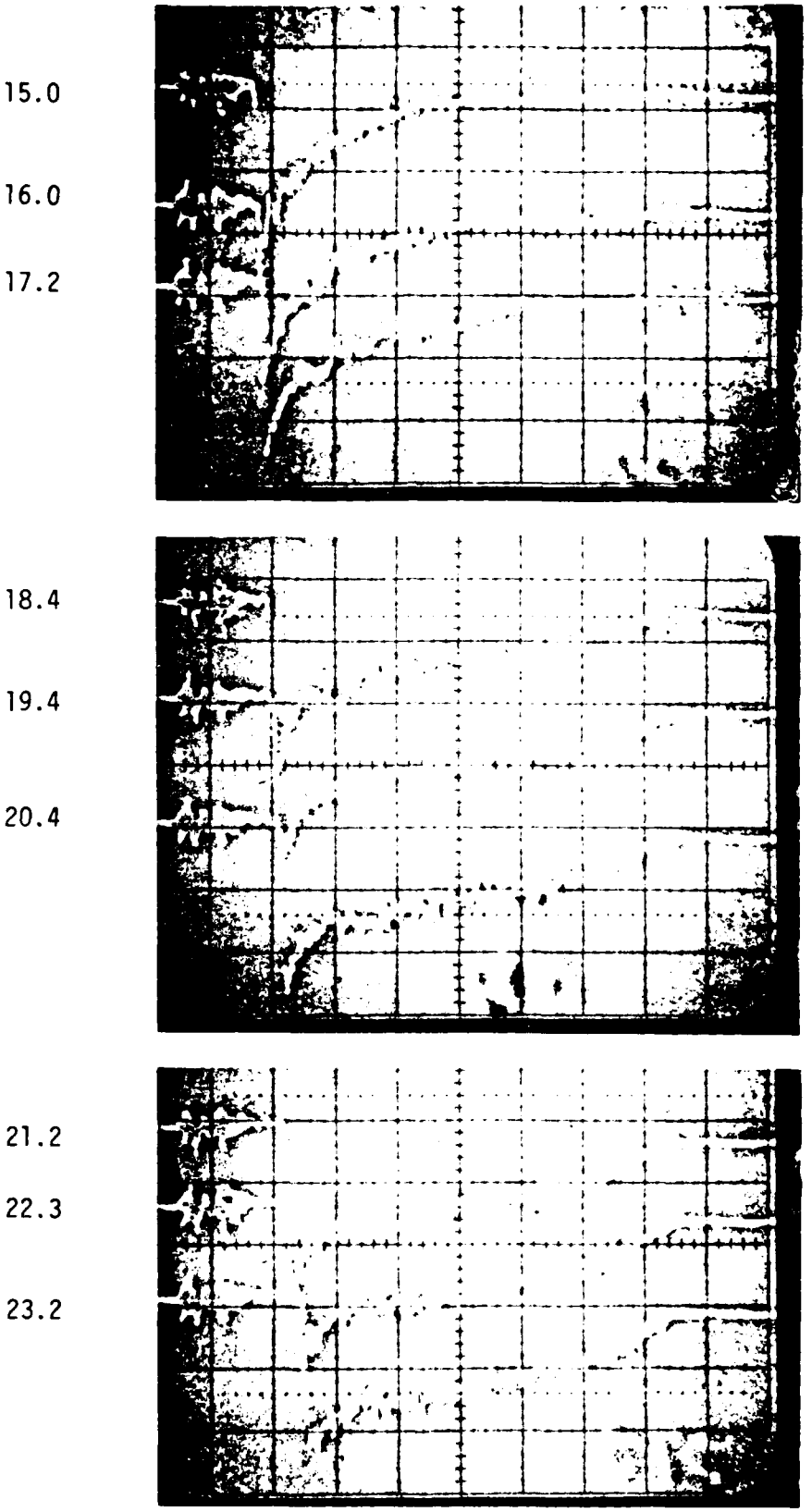

Figure C-9. Time history of 3577Å line emission for air breakdown at pressures from 15.0 to 23.2mmHg, fixed power.

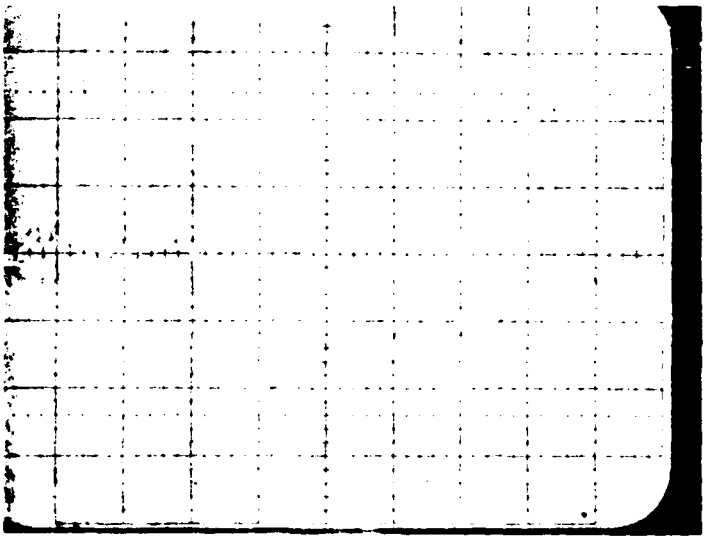

Figure C-10. Incident microwave power (top trace) and 3577A line emission (bottom trace) for air breakdown at 27.0 mmHg pressure. Horizontal scale is 1 μs/div.

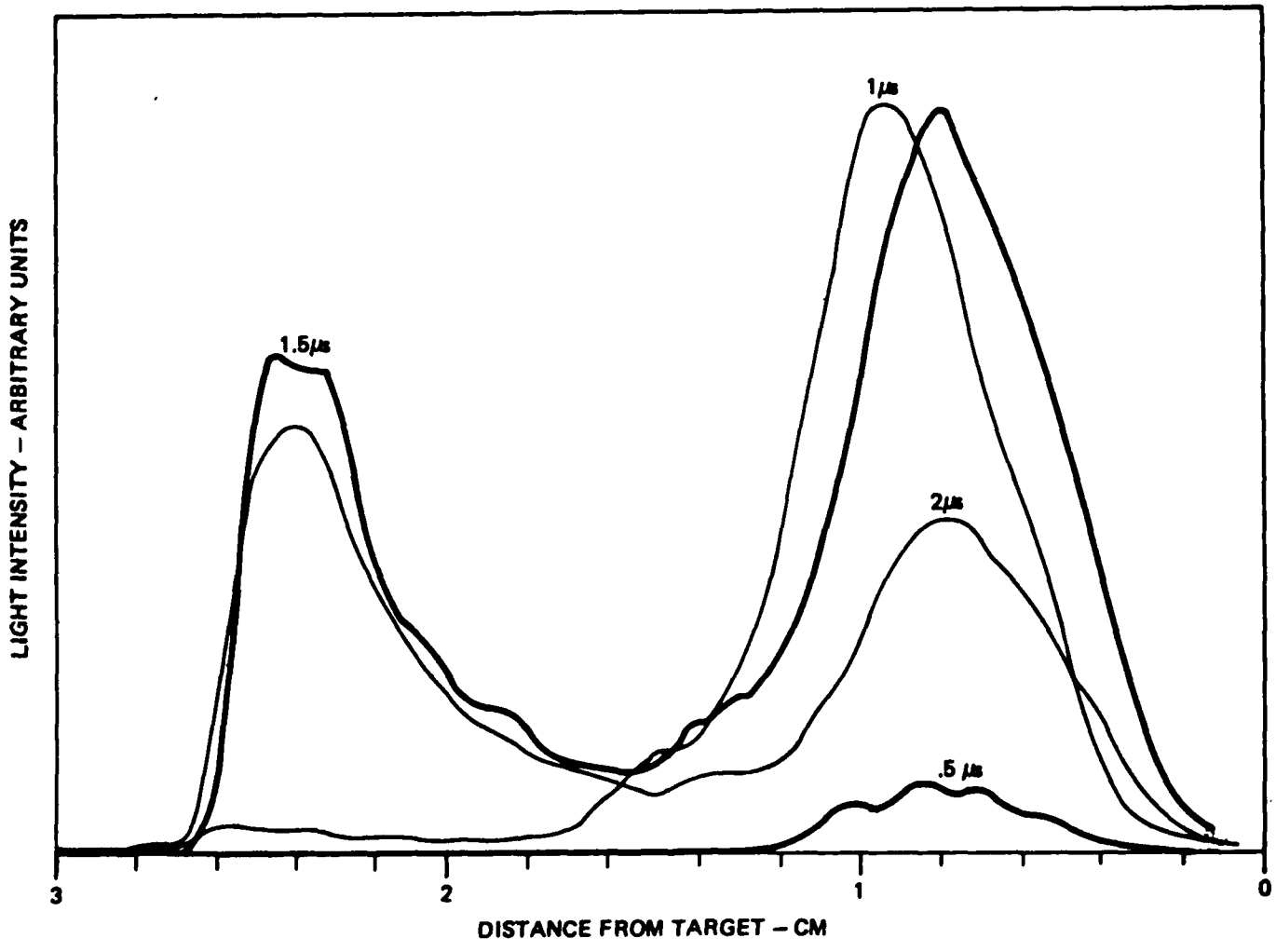

Figure C-11. HeI 5876A line intensity as a function of distance from target at various times during the microwave pulse. Helium fill pressure was 360 mmHg. Time resolution was .5 μs, determined by sampling gate width.

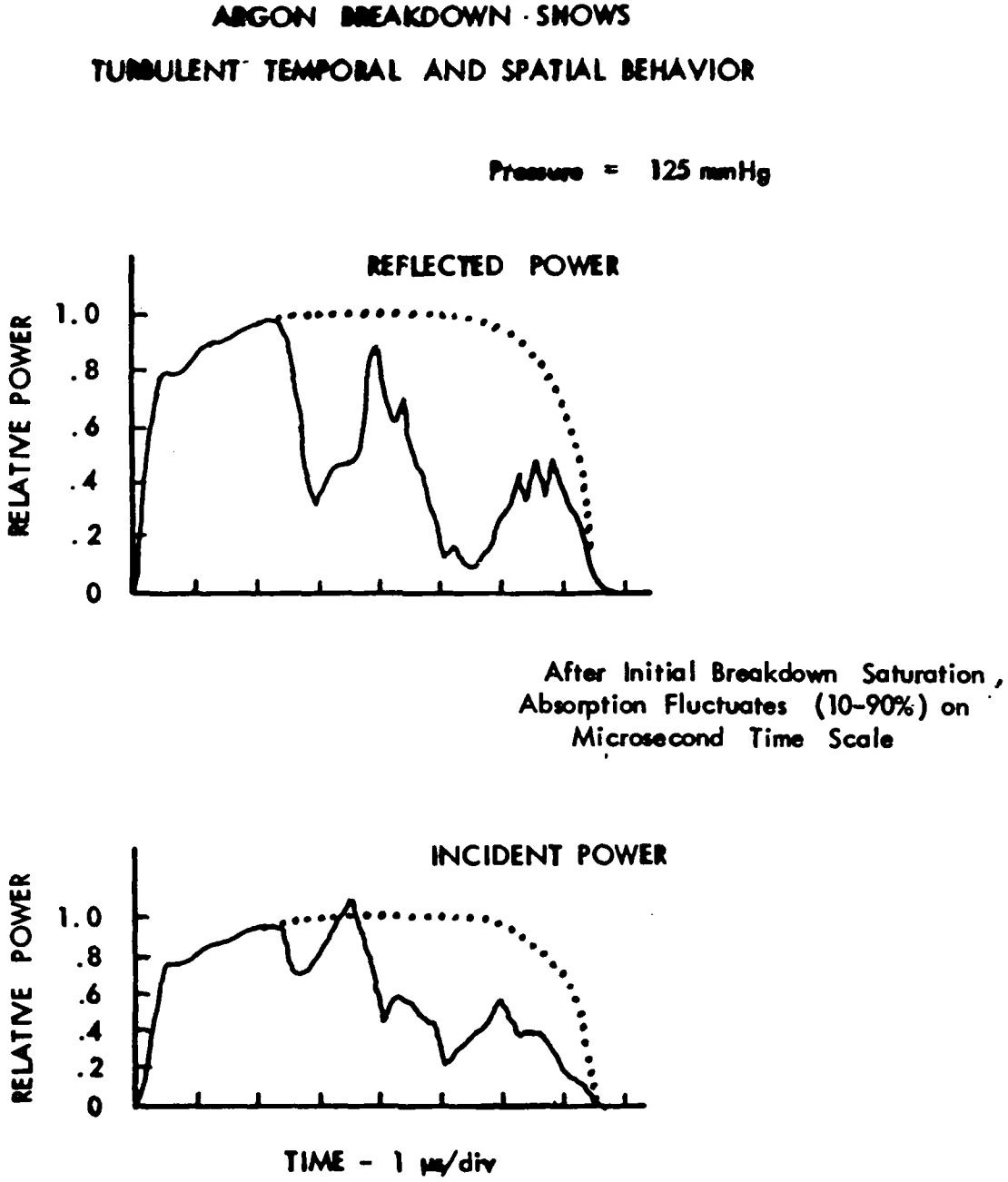

Figure C-12. Time history of power reflected from target/breakdown region (top graph) and power incident on target (bottom graph), for breakdown in Argon at fill pressure of 125 mmHg.

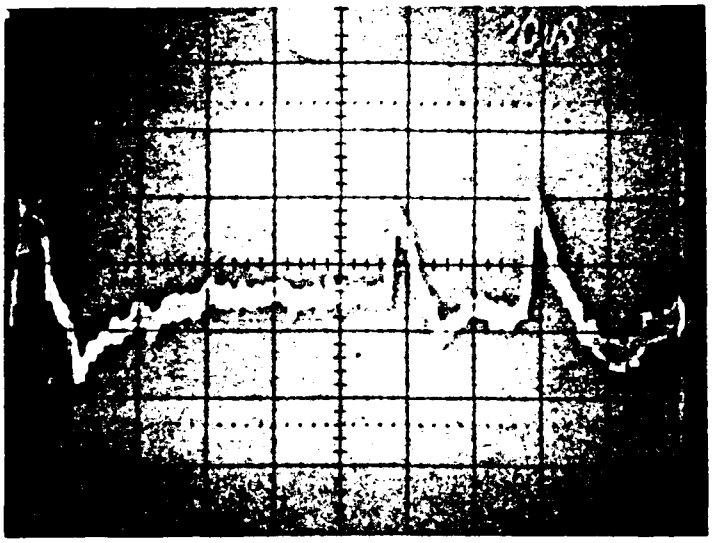

Figure C-13. Piezoelectric transducer signal at target surface for air breakdown at 25.3 mmHg. Horizontal scale is 20 µs/div., vertical scale 1 mV/div., corresponding to .05 psi/div. Characteristic rise time of the transducer was 1 µs.

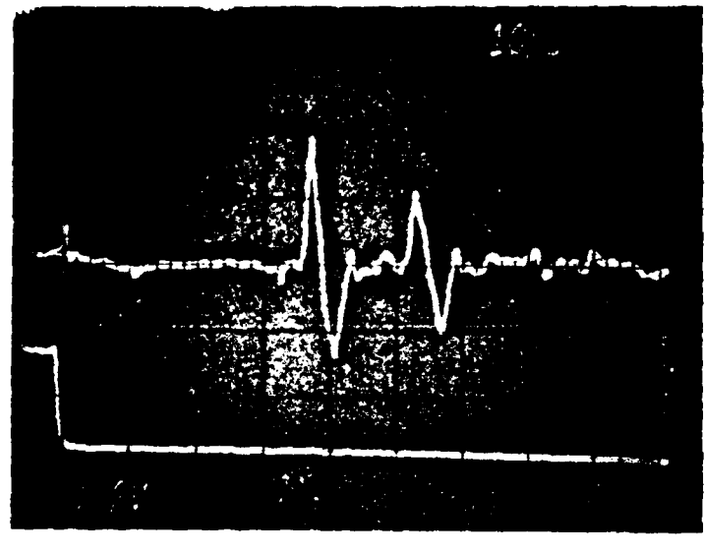

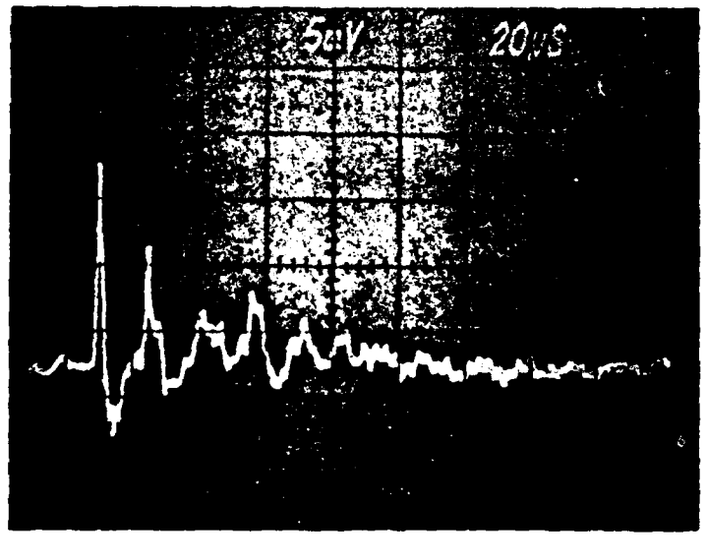

Figure C-14. Piezoelectric transducer signal at target surface for Helium breakdown at 480 mmHg (top photograph) and 330 mmHg (bottom photograph). In the case of the top photograph, there were two visible breakdown regions, and in the case of the bottom photograph, six. Veritical scale is 5 mV, or .25 psi, per division in both cases. Horizontal scale is 10 μs/div. in top photograph and 20 μs/div. in bottom.

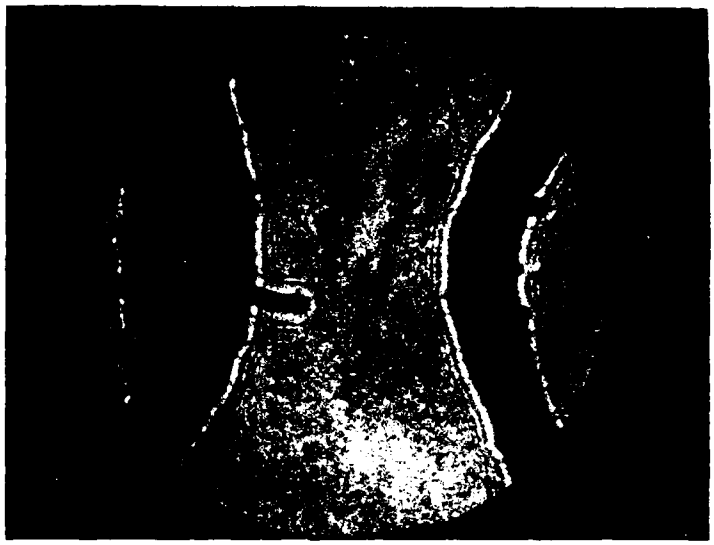

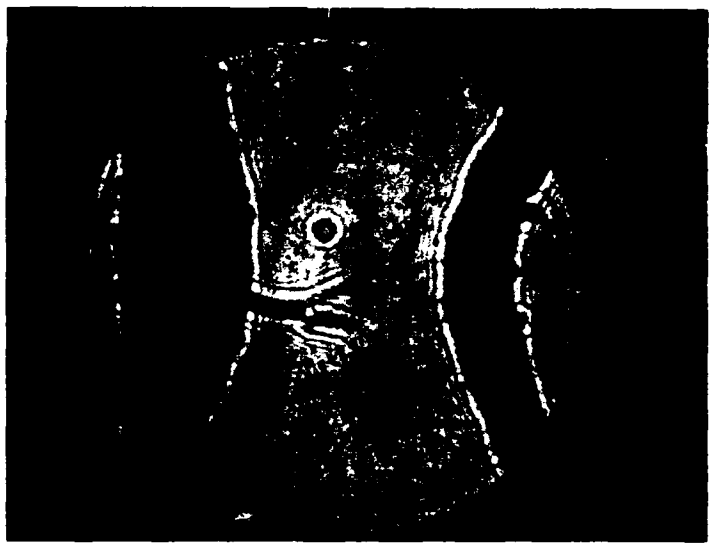

Figure C-15. Shadowgraphs of breakdown in waveguide like geometry at atmospheric pressure. Top photograph is without breakdown (t = 0), and shows copper mesh assembly and startup wire. In bottom photograph, .3 μs into microwave pulse, disturbance of air is visible at tip of startup wire.

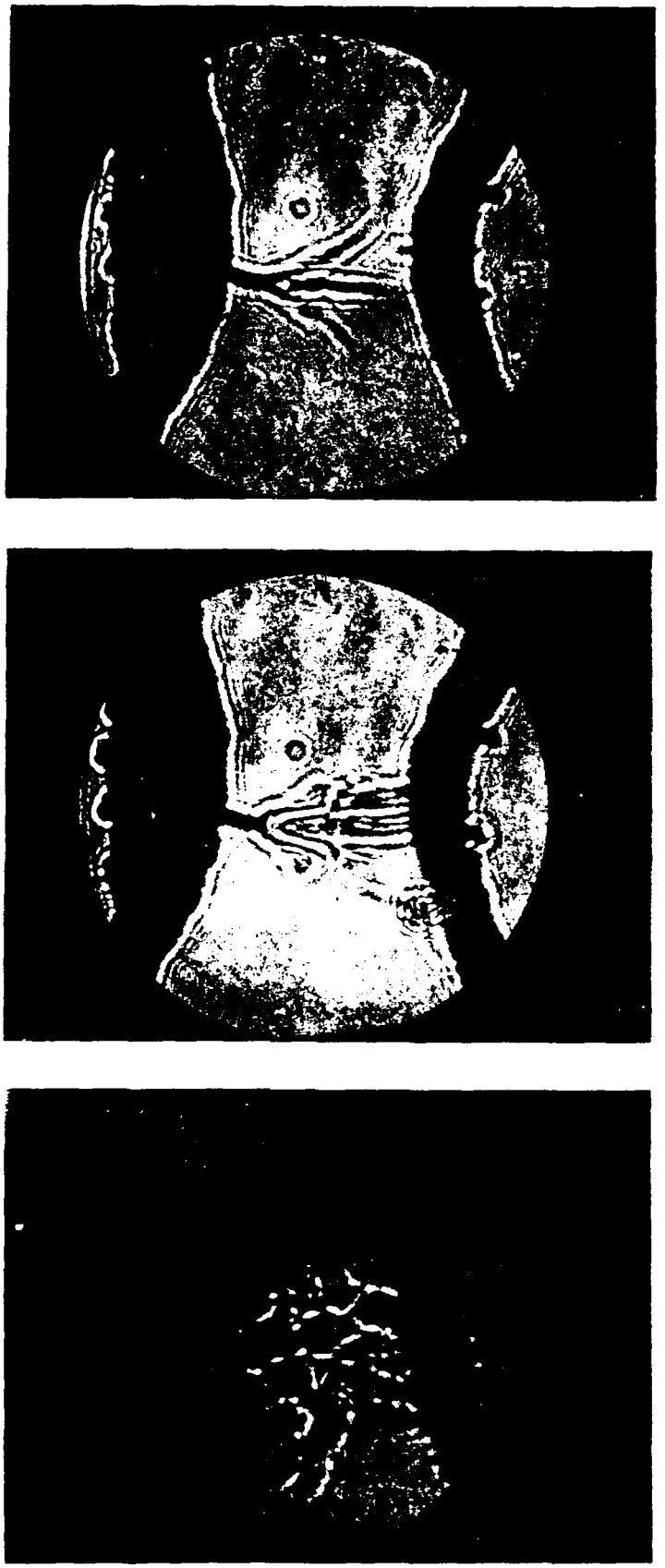

Figure C-16. Shadowgraphs at .6, 1.0 and 1.4 microseconds into microwave pulse, showing time development of breakdown.

END

3-87

DTIC